PERGAMON

Electrochimica Acta 47 (2002) 3571–3594

ELECTROCHIMICA Acta

www.elsevier.com/locate/electacta

Interfacial processes involving electrocatalytic evolution and oxidation of H_2, and the role of chemisorbed H

B.E. Conway [a,*], B.V. Tilak [b]

[a] *Chemistry Department, University of Ottawa, 10 Marie Curie Street, Ottawa, Ont., Canada K1N 6N5*
[b] *Process Technology Optimization Inc., 2801 Long Road, Grand Island, NY 14072, USA*

Received 15 February 2002; received in revised form 11 April 2002

Abstract

States of chemisorbed H that can be involved in the mechanism of the cathodic H_2 evolution reaction (HER) at metals, specially Pt, and the reverse oxidation reaction (HOR), are examined. Particular attention is paid to possible differences between underpotential-deposited (UPD) H, electrosorbed at potentials below the hydrogen reversible potential, and so-called overpotential-deposited (OPD) H that is involved, kinetically, as an intermediate in the HER. UPD H is involved in the HOR, following dissociative chemisorption of H_2, at potentials positive to the RHE potential. The roles of diffusion-control involving H_2, both in the HER and the HOR, are discussed in the light of experimental results for cathodic and anodic polarization. Values of exchange current-density, j_o, for the HER/HOR at equilibrium depend widely on the adsorptive and electronic properties of the metal, often representable as a 'volcano' relation with respect to metal-to-H bond energy. The origin of such relations, especially at the catalytic noble metals, is examined in terms of UPD and OPD states of H. Mechanistic and kinetic aspects of the HER and HOR are treated and their sensitivity to presence of CO and to surface structure at Pt single-crystal faces is reviewed. © 2002 Published by Elsevier Science Ltd.

Keywords: H_2 evolution reaction; Underpotential-deposited H; Overpotential-deposited H; H_2 oxidation

1. The electrochemical reactions of hydrogen: historical

The electrochemical reactions of cathodic H_2 evolution (HER) and anodic H_2 oxidation (HOR) have come to be regarded as archetypal processes in electrochemistry, especially in electrode-kinetics, serving as model examples for treatments of the latter. The electrochemical reactions involving hydrogen are of particular interest in regard to the involvement of atomic H in a chemisorbed state as an intermediate in the HER and HOR at electrode surfaces. Historically, it is well known that the concept of involvement of atomic H is one of the steps of H_2 formation in the electrolysis of water or acidic solutions, viz the $H+H \rightarrow H_2$ recombination step, as attributed to Tafel [1]. There are interesting relations of Tafel's H+H recombination mechanism of the HER to hydrogenation [2,3] and Bonhöffer's 'catalytic series' of metals for recombination of 2H to H_2 [4] where Pt lies high in the series yet H+H recombination is supposedly the rate-controlling step in the HER at Pt.

Tafel's interest in the hydrogen evolution reaction arose from his work on the electrochemical reduction ('electrochemical hydrogenation') of strychnine [2,3] and other organic molecules, carried out at Würzburg, following earlier co-authorships with Nobel prize winner, Emil Fischer. Interestingly, he observed that such reductions proceeded most efficiently at Pb or Hg, rather than at Pt where electrocatalysed cathodic H_2 evolution was the preferred process as a parallel reaction.

Of course, the primary historical episode in the course of the electrochemistry of hydrogen was the demonstration of electrolysis of water in 1800 [5] by Nicholson and Carlisle, using the voltage from a Volta pile.

* Corresponding author. Tel.: +1-613-562-5728; fax: +1-613-562-5170

0013-4686/02/$ - see front matter © 2002 Published by Elsevier Science Ltd.
PII: S0013-4686(02)00329-8

2. Types of reactions of hydrogen as H or H_2

The electrochemical reactions of hydrogen, as H or H_2, comprise the following types of process:

a) electrosorption of H, 2-d, at the catalytic noble metals, Pt, Rh, Ir, Pd and Ru, in the process of so-called underpotential-deposition (UPD) and its reverse, electrodesorption ionization, where electrosorbed H is already formed, e.g. at Pt, Rh, Pd, Ru, at potentials positive to the reversible potential of the hydrogen (H_2) electrode. The well known thermodynamic condition for UPD of H (and analogously for other UPD processes, e.g. metal ad-atom deposition) is that

$$G_{\mathrm{IL},\,\theta} < \tfrac{1}{2} G_{\mathrm{H_2}} \quad (1)$$

for some fractional coverage, θ_H, of the electrode surface where the Gibbs energies, G of the indicated species are not necessarily the standard-state values (cf. ref. [6]). Thus, chemisorbed H can be initially formed at the noble (catalytic) metals at low coverages before H_2 evolution can take place.Interestingly, the presence of UPD H at Pt was first indicated in the H-desorption, galvanostatic (dis-) charging curves for H at poly-crystalline Pt in the papers of Frumkin and Slygin already in 1933 [7]. Close inspection of their curves also reveals resolution of two distiguishable adsorption states of H, although that was not commented on at that time, nor was the term 'UPD' employed. However, cyclic voltammetry work, later [8], clearly resolved two, or even three distinguisable H chemisorption states at Pt(poly), dependent on co-adsorption of anions [9,10].

b) electrosorption and diffusion of H into host metals such as Pd, Ru, Ni and alloys such as Pd/Ag, $LaNi_5$ and a variety of other alloys;

c) dissociative electrosorption of H_2 with sorption of resulting H into catalytic metal hosts such as those in (b);

d) electrolytic evolution of H_2 by cathodic electron transfer from proton-donors such as H_3O^+, H_2O, CH_3OH, CH_3COOH, etc. with involvement of a chemisorbed H intermediate not necessarily in the same state of chemisorption of H as that in (a). This evolution of H_2 normally arises at finite overpotentials (η), i.e. at potentials negative to the reversible H^+/H_2 potentials (RHE); for such conditions, the adsorbed H intermediate is referred to as 'overpotential-deposited' (OPD) H in order to distinguish its conditions of formation (though not necessarily [see below] its state of adsorption) from those for UPD H;

e) electrocatalytic dissociative oxidation of H_2 at catalytic anodes, Pt, Rh, noble-metal alloys, etc, proceeding through steps that are usually the reverse of those involved in (d) and are thus involved in H_2-based fuel-cells; and

f) electrolytic hydrogenation of organics at cathodes such as Pt, Pd and their various alloys, proceeding via the agency of UPD or OPD H as the reducing agent generated in (a) or as the intermediate in processes arising in (d), or also in (b) or (c).

Understanding of the kinetics and mechanisms of the above processes, (a)-(f), requires knowledge and characterization of the states of UPD and OPD H at the noble, electrosorptive metals, and the chemisorptive behavior of H, and also the dissociative chemisorption of H from molecular H_2 at electrode potentials positive to the RHE potential at the pH of the electrolyte solution involved.

The process of UPD of H has received major attention in electrochemical surface science, especially in recent years at various (*hkl*) single-crystal surfaces of Pt [10,11] since the electro-chemisorption behavior of H has been found to be highly dependent on the 2-d geometry of e.g. Pt or Rh surfaces.

Formally, the UPD process is simple and is represented by, e.g., for acid pH,

$$\mathrm{Pt}(hkl) + \mathrm{H_3O^+} + \mathrm{e} \rightarrow \mathrm{Pt}(hkl)/\mathrm{H}_\theta + \mathrm{H_2O} \quad (2)$$

where H_θ represents a state of chemisorbed H at a fractional coverage, θ. Note that the bonding of H to Pt depends on the geometry (orientation index) of the Pt surface and also probably the extent of coverage owing to lateral surface-dipole interaction effects and the corresponding θ-dependence of the surface's electron work-function, Φ, [12,13]. Similar considerations apply to Rh and probably Ir, Pd and Ru. Polycrystalline Pt normally exhibits a mixture of H chemisorption behaviors, depending on the distribution of microfacets having various orientations, though usually mainly of the principal-index faces.

The surface electrochemistry of H at Pt has to be considered in the light of adsorption also of components of the electrolyte solution, e.g. the (usual) ubiquitous presence of water and of anions of the acid or salt also present. Perhaps surprisingly, in the early work of Breiter [14] and the later works of Jerkiewicz et al. [15], the enthalpy and standard Gibbs energy of chemisorption of H (calculated relative to $\frac{1}{2}H_2$) is little different from values [13] derived from gas-phase dissociative chemisorption experiments on $\frac{1}{2}H_2$. This suggests that the H atoms resulting from electrochemical UPD are little affected by the presence of H_2O dipoles above the H adsorption sites because the H atoms (in partially protonic states) reside in the structural holes or depressions that arise in obvious ways on the principal index faces; (note that on the (111) surface two types of

coordination holes are present, one with and another, adjacent, without a Pt atom beneath).

However, the following further points are to be noted with regard to the states of H at water-covered noble-metal surfaces that ubiquitously exist at electrode interfaces with solutions. Thermodynamic analysis [13,16] of the electrochemical and gas-phase adsorption of H shows that the enthalpy of formation of UPD H will be equal to the heat of adsorption of H, when the difference in the enthalpy of dehydration of the metal surface and the enthalpy of immersion of the metal is small. Experimental studies with Pt(111) surfaces have demonstrated (see ref. [13] for details) that H is bound to the Pt surface with an initial heat of adsorption of 46.8 kJ mol^{-1} which may be compared with the corresponding value of 41.2 kJ mol^{-1} based on UHV investigations. However, the adsorption energy decreases linearly with coverage for UPD H, while it is approximately constant up to a H-to-Pt atom ratio of 0.5 in UHV studies, leading to the suggestion that possible interactions of adsorbed H at a Pt/solution interface involve water.

It may be noted that the MH bond enrgy on transition metals varies only by $\pm 10\%$, while the heat of adsorption of UPD H on Pt is greater than on any other metal. Furthermore, many metals that strongly absorb H, e.g. Ti, Ni, Fe, do not exhibit any UPD of H electrochemically. These observations suggest [13] that the UPD H on platinum and related surfaces is a unique species and that thermodynamic data obtained from electrochemical UPD measurements [15], where solvent water is present, may not refer to the same state as corresponding data derived from UHV studies. In the examples where gas-phase H is strongly bound to transition metals such as those above, yet UPD of H is not observed is probably due, as at Ni, to oxide-film formation setting in already over the potential range where UPD of H might be expected to arise.

Much stronger and surface-specific interactions arise, however, on account of co-adsorption of anions such as HSO_4^-, ClO_4^-, OH^-, borate and halides. Effects of HSO_4^- relative to ClO_4^- have been studied in detail by means of comparative cyclic voltammetry and charge-displacement transients generated by competitive adsorption by CO [10,17]. The latter procedure has enabled the CV profile at Pt(111) in aq. H_2SO_4, over the potential range 0.05–0.35 V, to be resolved into two components: one due to UPD of H, corresponding to approximately 2/3 of the nominal monolayer H UPD charge and the remaining 1/3 associated with chemisorption of HSO_4^- ion (Fig. 1), viz formally:

$$Pt(111) + HSO_4^- \rightarrow Pt(111)/HSO_4 + e^-(\text{in Pt}) \qquad (3)$$

In this process, HSO_4 occupies three sites on Pt(111) per original anion, in trigonal symmetry.

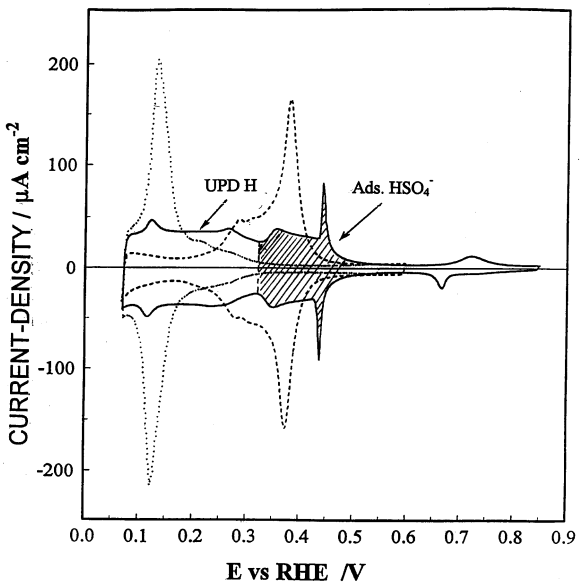

Fig. 1. Cyclic voltammograms for Pt(111) illustrating charge response region of ca. 33% due to HSO_4^- chemisorption in distinction from that for UPD H and in relation to voltammograms for (100) and (110) surfaces (from refs. [10,31], by permission of the publishers).

Somewhat similar, but smaller, competitive chemisorption between HSO_4^- and H arises at the (100) surface as indicated by impedance spectroscopy results obtained by Morin, Barber and Conway [18], illustrated in Fig. 2, compared with a normalized cyclic voltammogram.

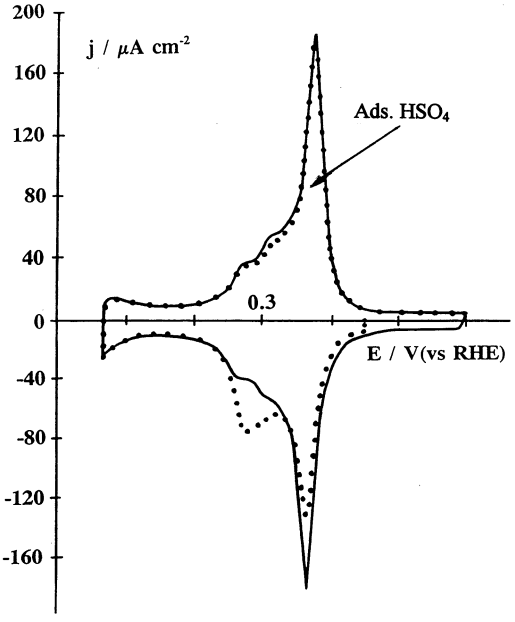

Fig. 2. Impedance spectra results (points) for Pt(100) in aq. H_2SO_4 response (from refs. [18,75], with permission of the publishers).

3. Thermodynamic functions for UPD of H and metal-to-H bond energies

3.1. The Gibbs energy

The primary function is $\Delta G_{H,UPD}$ or the corresponding standard value, $\Delta G^{\circ}_{H,UPD}$. It is directly derivable from cyclic voltammetry, e.g. at Pt, from voltammograms recorded using an hydrogen reference electrode, which give a range of values depending on coverage, θ_H. On this scale, the $\Delta G_{H,UPD}$ is related to the experimental potentials, E_H, on that scale by $E_{E,UPD} - E_{1/2H_2} = -\Delta G_{H,UPD}/F$. For Langmuir chemisorption of H, the standard-state is $\theta_H = 0.5$. When lateral interactions are significant, as at Pt(111), special definition of the standard-state has to be given according to the analysis of Conway and Dhar [6].

The $\Delta G_{H,UPD}$ is related to the Gibbs energy of electrode-to-H (M–H) bonding through the processes:

$$\tfrac{1}{2}\,H_{2,g} + M \rightarrow M\text{–}H \quad (4)$$

$$\tfrac{1}{2}\,H_{2,g} \rightarrow H_g \quad (5)$$

and

$$H_g + M \rightarrow M\text{–}H \quad (6)$$

where M is a surface site at the metal interface.

3.2. The enthalpy of electrosorption of H

The standard entropy of UPD H can be determined (see Section 3.3 below) from the temperature-dependence of $\Delta G^{\circ}_{H,UPD}$ which, combined with $T\Delta S^{\circ}_{H,UPD}$, gives the corresponding $\Delta H^{\circ}_{H,UPD}$ and thence the metal-to-H bond energy corresponding to process (Eq. (6)). Significantly, as first found by Breiter [14], and subsequently derived for single-crystal Pt surfaces by Ross [19] and later by Zolfaghari and Jerkiewicz [15], the M–H bond energy at Pt electrodes is quite similar to that evaluated for gas-phase adsorption of H as noted in the articles by Ross [15] and by Christmann [13]. This implies, of course, that the ubiquitous presence of water at electrodes (in aqueous solution) has little effect on the binding energy of H, though FTIR surface spectroscopy (Ref. [27], Section 7.3) indicates H-bonding between UPD H and adsorbed H_2O (see Section 7.3).

It seems that the first voltammetric and thermodynamic study of UPD of H on single-crystal planes of Pt, (100), (110) and (111), was that of Will [21] although he recognized that each of his crystal faces exposed more than one individual plane; also, the surface roughness factors were appreciable, 1.0–2.4, and changed with potential cycling in cyclic voltammetry experiments. Also, restructuring of the surfaces took place on extended cycling. The use of 8 N H_2SO_4 in this work, as we now know, would have led to appreciable effects on the UPD profiles of adsorbed H relative to the behavior in dilute H_2SO_4 or $HClO_4$. Thus the results differ qualitatively from the later, now classical, profiles of Clavilier et al. [10] on well ordered single-crystal Pt surfaces. Temperature effects (0–80 °C) were studied, for the first time, on the three principal-index planes but their interpretation is complicated by the co-adsorption of HSO_4^- ions.

Notably, the results of this work [19] enabled the heats of adsorption of H on the three surfaces to be determined by the procedure of Breiter et al. [14,22] which the latter authors applied at polycrystalline Pt. The enthalpies of electro-chemisorption of H were found to decrease in the order (100) > (111) > (110), except for H coverages > 80%. Generally, the heats of adsorption decreased appreciably, by 50–60%, with increase of H coverage from 5 to 80%. The trend of these results was also consistent with the then available gas-phase results of Aston [23] and later results referred to by Christmann [13].

Ross [19] has made a detailed examination and review of H electrosorption on single-crystal Pt surfaces using an in situ LEED–Auger system with transfer capability to or from an electrolytic cell based on the technique of Hubbard et al. [24]. Thermodynamic functions for H adsorption at the (111) and (100) surfaces, derived from temperature-dependent studies, were evaluated with the following results:

Pt Surface	ΔG°_{ads} (kJ mol^{-1})	ΔH°_{ads} (kJ mol^{-1})	ΔS°_{ads} (J K^{-1} mol^{-1})	U_{11} (kJ mol^{-1} per mol-pair)
(111)	−30.1	−46.8	−55.8	5.0
(100)	−65.2	−81.1	−53.1	5.0

where U_{11} is a pair-wise lateral interaction energy accounting for the decrease of energy of H adsorption with increasing fractional coverage, as recognized in the paper of Will [21].

The question of comparison of ΔH_{ads} at Pt in solution with corresponding gas-phase values has been considered by various authors [13–15,19,22]. The initial (zero coverage) heats of adsorption for single-crystals of Pt have been reported by McCabe and Schmidt [25] to be 73.2 kJ mol^{-1} for (111) and 102.4 kJ mol^{-1} for (100) with a U_{11} value of 13.2 kJ mol^{-1} per mol-pair. Ertl et al. [26], however, have found much smaller values for H on Pt (111), 41.2 kJ mol^{-1}, and shown that larger values arise if (111) crystals are poorly annealed, then giving a value of 67 kJ mol^{-1}.

Generally, the conclusion is that because H_2O interaction with Pt surfaces is weak, the ubiquitous presence of co-adsorbed H_2O molecules at electrodes has little influence on the adsorption energy of H [13,15,19,22]. Also, the H atom or 'partial ion' is very small and can be accommodated with little steric competition with water molecules.

3.3. The entropy of underpotential-deposited H

The standard entropy of UPD H (S°_{H}) is of interest with regard to whether the chemisorbed H is mobile in 2-d or immobile. For the latter situation, the S°_{H} would be expected (cf. refs. [27,28]) to be substantially smaller than that of mobile adsorption. By conducting CVs over the H UPD potential range at Pt at various temperatures, Conway, Kozlowska and Sharp [28] plotted UPD peak potentials versus temperature and derived S°_{H} values for the chemisorbed H derived from H_3O^+ discharge. This can be done in two ways: (i) obtaining the T-dependence of peak potentials versus the RHE potential in the same solution (in an isothermal cell) with thermodynamic correction for the absolute T-dependence of the RHE potential based on the single-ion proton partial molal entropy and the known standard entropy of $\frac{1}{2}H_2$; (ii) by similar measurements in a non-isothermal cell with corrections (cf. ref. [29]) for the thermal liquid-junction potential across the temperature gradient. A third way [28] is to directly measure the UPD H peak potentials relative to the RHE potential in an isothermal cell at various temperatures. Then the ΔS° for H chemisorption can be derived directly from the standard ΔS value for the process

$$2Pt/H_{\theta} \rightarrow 2Pt + H_2 \quad (7)$$

for a given fractional H coverage, θ, and its potential relative to that of the RHE involving the H_2 in Eq. (7) above.

From their voltammetry results at various temperatures, Conway et al. [28] were able to distinguish clearly the state of surface mobility or otherwise of UPD H at Pt (poly) from analysis of results based on dissociative chemisorption from $\frac{1}{2}H_2$ at the Pt (poly) electrode; they found $\Delta S^{\circ}_{H,UPD} = -84$ to $-73(\pm 8)$ J K^{-1} mol^{-1}, but dependent on the UP H ionization peak in voltammetry. The above results clearly indicate immobile adsorption according to a statistical–mechanical calculation [28] where the $\Delta S^{\circ}_{H,UPD}$ would be only -8.8 J K^{-1} mol^{-1} for mobile adsorption. They also observed anomalous entropy behavior of the middle UPD H peak at Pt, which they attributed to effects of chemisorbed HSO_4^- ion [[28]; cf. Ref. [10]], subsequently confirmed by voltammetry and radio-tracer measurements.

More recently, experiments of a related kind were performed by Jerkiewicz and Zolfaghari [15,30] on the entropy of UPD H at single-crystal Pt surfaces based on the method of Breiter [14] using a thermodynamic cycle via an hypothetical equilibrium between adsorbed H at coverages, θ_H, and H_2 gas fugacity. Several of their results are recorded below which illustrate the dependence of $S^{\circ}_{H,\theta}$ on coverage, θ_H, and on the index of the single-crystal Pt plane. These results are complementary to those earlier determined by Ross [19], referred to in Section 3.2, and by Conway et al. [28]..

For Pt(111) in 0.05 M H_2SO_4, over the coverage range $0 < \theta_{H,UPD} < 2/3$, $\Delta G^{\circ}_{H,UPD}$ varies from -26 to -8 kJ mol^{-1} and the derivative quantities, $\Delta S^{\circ}_{H,UPD}$ from -79 to -63 J K^{-1} mol^{-1} and $\Delta H^{\circ}_{H,UPD}$ from -44 to -30 kJ mol^{-1}. The energy of lateral repulsion is 27 kJ mol^{-1} corresponding to a value of the g factor in the Frumkin isotherm of ref. [11]. For Pt(poly) $\Delta S^{\circ}_{H,UPD}$ was evaluated [5,30] as -70 J K^{-1} mol^{-1} in moderate agreement with the value of Conway, Kozlowska and Sharpe of -83 to -74 J K^{-1} mol^{-1} [28].

From these $\Delta S^{\circ}_{H,\theta}$ data and corresponding $\Delta G^{\circ}_{H,\theta}$ from the voltammograms, these authors derived the bond energies of H to Pt and their decrease with H coverage [30]. Like Breiter [14], they found values similar to those for chemisorption from gas-phase H_2, allowing for the dissociation energy of $\frac{1}{2}H_2$ in Eq. 5. Similar conclusions were reached by Christmann [13].

4. Relations to dissociative adsorption from gas-phase H_2

As noted in Section 3.2, it was already evident from early works of Breiter [14,22] and that of Ross [19], referred to above, that the bonding energy between electrosorbed H at low coverages and Pt surfaces was little different from that evaluated for dissociative adsorption from gas-phase H_2, allowing for the dissociation energy of molecular H_2.

A detailed review on the states of adsorbed H at a variety of metals, including single-crystal Pt surfaces, was given by Christmann in 1998 [13] covering comparisons between H dissociatively chemisorbed from gas-phase H_2 and electrochemically deposited H. The results discussed were principally focussed on data derived by use of temperature-programmed thermal desorption (TPTD) which gives information analogous to that obtainable at electrodes by means of cyclic voltammetry at low sweep-rates in the sense of distinguishing differently bound states of adsorbates, here H. However, the resulting 'desorption spectra' are not strictly thermodynamic in significance as are the desorption potentials from slow voltammetry [28]. However, TPTD spectra show distinguishable bound states even at single-crystal surfaces, as does voltammetry [35,39], e.g. for Pt (100).

An important complication arises in that the act of chemisorption of H itself can lead to reconstruction and thence to apparent different binding energies as also arise from distributed defect sites [13]. There is also the effect of 'induced heterogeneity' (a term applied by Boudart [12] to effects of local coverage on the surface's work function) which can lead to changes of H binding energy with increasing θ_H as illustrated in Fig. 1 three of Christmann's review [13]. A related heterogeneity effect

was proposed by Conway and Kozlowska [39] through calculations of relative energies of successive 2-d overlay array structures that can develop on single-crystal lattices with increasing θ_H.

In cyclic voltammetry of the Pt(111) surface, about 66% of coverage by H is laid down with a pseudocapacitance, C_ϕ, that is almost constant over a potential range of approximately 0.3 V, apparently indicating (cf. Ref. [33]) a large Gibbs energy of lateral interaction with increasing θ_H. However, the observed H capacitance on Pt(111) [11] is too large and arises over too small a range of potential to be consistent with the apparent 2-d interaction parameter (g in ref. [33]). It was, therefore, suggested by Conway [34] that the three 'Langmuirian' C_ϕ peaks [31,32], developed with increasing potential, are associated with successive occupancy of substrate overlay lattices as $0 < \theta_H < 1$, the net, additive, result being then an almost linear relation of θ_H with increasing potential (C_ϕ constant).

Note that the remaining 33% of charge at Pt(111), towards nominal monolayer occupancy, is associated with chemisorption of HSO_4^- ions of the electrolyte with e-transfer (see refs. [10,17]). Some co-adsorption of HSO_4^- also arises at Pt(100) [18].

Notionally (Fig. 3), completion of the H monolayer can be envisaged as taking place beyond the hydrogen reversible potential, as indicated by the second hatched region in Fig. 3.

The decline of adsorption energy of H with increasing θ_H [30] seems to be a general phenomenon, also found for gas-phase chemisorption of H from $\frac{1}{2}H_2$, e.g. for Rh(110) [35] and Ni(110) [36], as noted by Christmann [13].

5. Relation between UPD and OPD of H

Study of the states of UPD H, especially their specific relations to 2-d geometry of Pt or Rh single-crystal surfaces [10,11,15,30,37], has become an activity of major significance in recent electrochemical surface science. Complementarily, the relation between the states and coverages of UPD H relative to OPD H in the HER has become an interesting issue [38–40].

Formally speaking, UPD of H terminates at the hydrogen reversible potential from the direction of potentials positive to it, with coverages becoming smaller with increasing positive potential, while OPD of H commences at potentials negative to it.

However, this distinction evidently must depend [38] on the conditions determining the reversible potential of the HER, viz. especially the H_2 gas pressure (or fugacity) and/or the temperature, since coverage by UPD H is not normally dependent on H_2 pressure except at the H_2 reversible potential where UPD and OPD H are, by

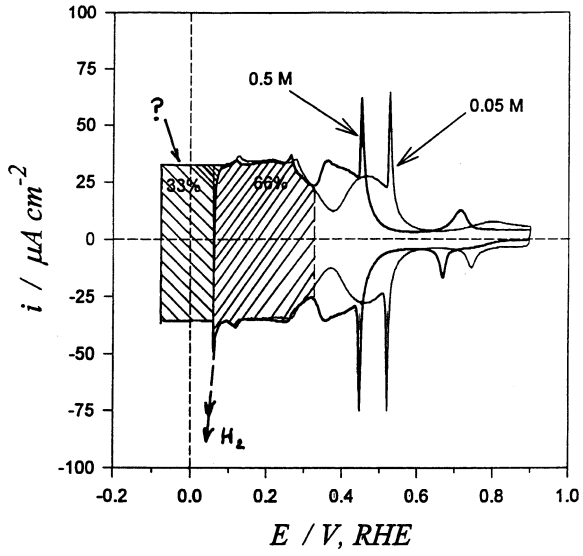

Fig. 3. Cyclic voltammograms for Pt(111) illustrating notional extensions of UPD H region formally into the OPD region, through the H_2 reversible potential.

definition, no longer distinguishable, or for the situation where UDP H coverage, θ_H, is determined (at hypothetical equilibrium at some H_2 pressure) by dissociative chemisorption of H_2 to $2H_\theta$ at say Pt. For example, under most conditions in CV experiments at, say Pt, pure Ar or N_2 is bubbled, so that H_2 fugacity $\rightarrow 0$. Then the equilibrium UPD potentials as $f(\theta_H)$ are determined by equilibria between UPD H at θ and H^+ ion or H_2O, rather than with H_2 gas.

Fig. 4 illustrates the situation for a series of four, arbitrary Lanmuir-type (cf. [40]) UPD H coverage isotherms as a function of potential, having different standard Gibbs energies, ΔG_H°, for electrochemisorption of H, plotted relative to the line for a given reversible

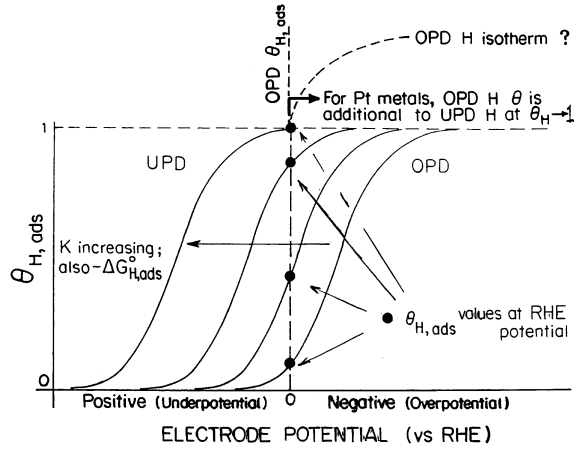

Fig. 4. Working diagram illustrating relation of several arbitrary Langmuir-type isotherm functions for UPD of H, for various values of ln K or $\Delta G_{H,UPD}^\circ$, in relation to the standard H_2 reversible potential (this diagram also illustrates, formally, the transition from UPD to OPD conditions for H electrosorption).

hydrogen (H_2) electrode potential. As ΔG_H° becomes more negative, UPD H coverages become larger at a given electrode potential and correspondingly greater at the HER reversible potential. At Pt, the negative ΔG_H° is sufficiently large that the UPD H coverage, θ_H, already attains a value near unity at that potential except for the (111) surface where approximately 33% of accessible Pt surface sites are already occupied by chemisorbed HSO_4^- anions [10,17]. At that surface, further occupancy of sites can only arise at potentials sufficiently negative to the H_2 reversible potential that cathodic desorption of HSO_4^- takes place formally at negative overpotentials, i.e. into the OPD H adsorption region. This situation was illustrated schematically in Fig. 3.

For the situations illustrated in Fig. 4, for sufficiently appreciable values of $-\Delta G_H^\circ$, that $\theta_{H,UPD}$ already = 1 at the H_2 reversible potential, the question arises how the extra OPD H ($\theta_{H,OPD}$) is to be accommodated: it could be bonded atop of Pt atoms with the UPD H residing in coordinatively more complex sites, e.g. in the declevities between 3 (on(111)) or 4 (on Pt(100)) coordination sites. This would imply distinguishably different bonding sites for UPD and OPD H. At the Pt(111) surface, note that for $\theta_{H,UPD} \rightarrow 1$ at $q_H = 210$ μC cm^{-2}, there still remain an equal number of coordinatively different sites, so that OPD H could increasingly occupy those sites as $-\eta$ increased. Horiuti and Toya [41] suggested such a possibility for the difference between the weakly and strongly bound H (Fig. 3).

Alternatively, for accommodation of OPD H beyond $\theta_{H,UPD} \rightarrow 1$ at Pt or Rh, a new communal array arrangement of both UPD and OPD H could become established [38] having a common value of $-\Delta G_H^\circ$, different from that for the UPD H electrosorbed below the H_2 reversible potential, and a non-commensurate 2-d structural relation to the metal surface.

For appreciable pressures of molecular H_2, the reversible potential becomes more negative in proportion to $-RT/F \ln p_{H_2}^{1/2}$ (relative to its standard value for $p_{H_2} = 1$ atm), so that coverage by H, designated as UPD H, can be extended to larger values into a potential range that was designated as for OPD of H for the standard potential condition (cf. Fig. 3). Thus, the distinction of what is to be regarded as UPD or OPD H becomes thermodynamically rather arbitrary, a point that has not been well recognized previously except in our own earlier discussion of this point [38].

The H_2 reversible potential is, of course, also dependent on ln a_{H^+} or $\sim -$pH. However, this factor will not affect the range of UPD, relative to onset of OPD of H, since both processes follow the same dependence on pH.

The situation at other electrode metals having less strong affinities for H, i.e. smaller $-\Delta G_H^\circ$ values, corresponds to the positions of the H isotherms in Fig. 4 more to the right along the potential axis. For such cases, the fractional coverage, $\theta_{H,UPD}$ at the H_2 reversible potential can (see Fig. 4) be less, or much less, than 1. Then, as the potential is increased through the H_2 reversible potential, to negative η values, there can be a continuous change from a UPD to a formally OPD state of H as adsorbed H becomes the intermediate in the mechanism and process of cathodic H_2 evolution. Note, however, that this transition, being only a formal thermodynamic one, does not correspond, in this case, to a chemically or coordinatively different bonding of the OPD H from that for the UPD H deposited below the reversible potential, as is the case at Pt.

The cases of cathode metals such as Ni or Co are of interest. Their well known chemisorptive properties for H and their log j_o values (see Section 9) would lead to the expectation that they would exhibit observable UPD of H when used as electrode materials. However, this is not the case; the reason seems to be that over the potential range expected for UPD of H (+0.05 to +0.35 V, vs. RHE), surface oxidation sets in with oxide-film formation (see potential/pH Pourbaix diagrams for Ni and Co) arising over that potential range so that no H chemisorption can be detected electrochemically, e.g. in cyclic voltammetry [42], although OPD H coverage can be evaluated (Section 7 [43]).

6. Reaction steps in mechanisms of the HER and the involvement of adsorbed H

6.1. Reaction steps

The following are the now generally accepted [44,45] steps by which cathodic H_2 evolution occurs at various metals, M, involving an adsorbed H intermediate, MH_{ads}:

$$H_3O^+ + e^- + M \rightarrow MH_{ads} + H_2O \quad \text{Step I}$$

followed either by:

$$MH_{ads} + H_2O^+ + e^- \rightarrow H_2\uparrow + H_2O \quad \text{Step II}$$

or:

$$2MH_{ads} \rightarrow 2M + H_2\uparrow \quad \text{Step III}$$

In acidic media, H_3O^+ ion is the proton source for the initial discharge step I while in alkaline solution or for pHs > approximately 5, H_2O itself is the proton source leading to OH^- as the conjugate-base product after electron transfer.

The steps above are often distinguished by names: I, the Volmer step; II, the Heyrovsky step and III the Tafel step (another step, involving an H_2^+ ion [well known in radiation chemistry] intermediate, had been suggested by Horiuti).

The adsorbed H intermediate (MH_{ads}) in I, II and III is what has been referred to above and in recent

literature [38–40] as 'OPD H'. This intermediate is chemically identical with 'UPD H' but its surface coordination, e.g. on Pt, Rh, etc and single-crystals thereof, and its electronic environment, can be different from that of UPD H, depending on cathode metal and electrode potential in relation to potential-dependent electron-spill-over [46,47] at the metal surface into the double-layer.

The distinction between steps I, II or III as possible rate-controlling mechanisms in the HER in terms of Tafel slopes (b) and steady-state coverages (θ_H) is now classical in the literature [44,45], as is recognition that steps II or III are alternative desorption steps for H_2 formation but each is consecutive with respect to step I. The kinetic conditions with respect to rate constant and potential-dependence of coverages by (OPD) H for identification of rate-determining steps and reaction pathways have been treated in detail in earlier literature [45,46]. Generally, when step I is rate-controlling, θ_H values tend to be small or very small (as for the HER at Hg, Tl and Pb) while if steps II or II are rate-determining, θ_H can be appreciable, but this depends on the potential-dependent quasi-equilibrium constant for step I at various metals when step I is not rate-controlling. Of course, the overall θ_H can be large at these noble metals at which UPD of H arises (see Section 5 above) but the extra, kinetically involved, coverage by OPD H is potential dependent (see Eq. 8 above and Eq. 15 below).

6.2. Tafel slopes, b, and their temperature dependence

Limiting values of Tafel slopes, b, for steps I, II and III, based on an assumed barrier symmetry factor β, $\simeq$ 0.5 (as found at Hg for 298 K in non-specifically adsorbed electrolyte where $b \simeq 118 \pm 2$ mV) provided diagnostic criteria [44,45] for distinction of mechanisms of the HER in relation to potential-dependence of OPD H coverages, $\theta_{H,OPD}$, as follows:

Step	Low $\theta_{H,OPD}$ (mV)	Higher, η-dependent $\theta_{H,OPD}$ (mV)
I	−118	$-(\theta_{H,OPD} \ll 1)$
II	−118	−42
III	−29	$\rightarrow \infty$ (limiting current)

More generally, since $\theta_{H,OPD}$ is determined by a potential-dependent electrosorption isotherm [33], b has the form:

$$-1/b = \frac{F}{RT}\left(\beta + \frac{RT}{F}\, \mathrm{d}[\ln \theta_H]/\mathrm{d}\eta\right) \quad (8)$$

It should be noted that a majority of studies lacks supporting information pertaining to the coverage, θ_H, except by Conway's school [48,49] which has provided data on potential-dependence of H coverage during the HER, employing an analysis of potential-decay transients following current interruption, supporting the mechanistic conclusions based on an analysis of the steady-state data and complementarily, impedance data. It is essential that such information be sought for unambiguously elucidating reaction mechanisms and their possible changes with potential.

Most mechanistic postulates assume that a single rate-determining step, rds, prevails during the course of the HER. Based on radio-tracer studies and stoichiometric numbers for the HER on various substates, Enyo [50,51] has questioned the concept of a unique rds. His observations reveal that the ratio, r, of the exchange current-density of the discharge step to that of the recombination step is close to 1 on Rh and Ni, even though the shapes of the polarization curves suggest a unique rds.

This leads to the suggestion by Enyo that the 'affinity' of the reaction (the ΔG change) could be equally apportioned between two steps involved during the HER and, therefore, these steps can proceed with almost the same j_o values. However, kinetic studies using Enyo's procedure are scarce while other data-fitting methods seem more productive, e.g. via impedance spectroscopy.

An important and curious observation during the course of work on the HER has been the observation of low Tafel slopes [52,53] on high surface-area porous electrodes. Thus, as shown in Figs. 5 and 6, Pt and Ni exhibit low Tafel slopes as the specific surface area/porosity of the coating increases. This is not simply a consequence of resulting low current-densities (on a real-area basis), as the low Tafel slopes prevail even at $-\eta$ values of >100 mV. The low Tafel slopes could arise as a result of participation of a different state of the H intermediate, promoted by the disordered state of the metal in Raney-type materials or electrodeposited composites such as Ni–Mo–Cd, associated with OPD H sorption. However, the nature and the chemistry of the intermediate is not obvious. Alternately, it is possible that the low Tafel slopes are, for some reason, a result of the HER occurring on a highly porous matrix. Theoretical calculations [54a] assuming a homogeneous model for the porous substate show that when an electron-transfer step is rate-determining, one should expect doubling of Tafel slopes at high overpotentials, whereas when a chemical step is rate-controlling, j is proportional to $-\eta$ and no limiting Tafel behavior arises. If, on the other hand, diffusion of H_2 from the electrode surface to the bulk of the solution is assumed to be slow and when the activation polarization is negligible (i.e. $j_o \rightarrow \infty$), it was shown [54,55] that a Tafel slope of $0.8RT/F$ at low overpotentials and $2RT/F$ at high overpotentials can prevail. These values may be compared with the value of $RT/2F$ expected on planar electrodes for the same mechanism. It is unlikely that

diffusion of H_2 in solution is the 'slow'-step during the course of the HER due to its low solubility in concentrated NaOH or KOH solutions. Furthermore, this behavior was never observed on planar electrodes during the course of the HER.

The above discussion of b values is based on the assumption that β for the charge-transfer steps I and II are both independent of potential and temperature. However, following the suggestion of Agar [54] that the entropy of activation could be a potential-dependent component of the Gibbs energy of activation, $\Delta G^{\circ\ddagger}$, Conway, MacKinnon and Tilak [55] showed that Tafel slope values for the HER at Hg and Ni, determined over a wide range of temperature, T, were not simply $2.3RT/\beta F$ but could be independent of T (i.e. β was linear in T) or contain at T-independent term, $b = 2.3RT/\beta F + K$. Similar conclusions were reached by Yeager et al. [56] for the anodic O_2 evolution reaction studied over a range of T. Conway et al. [55] suggested that the overall β for charge transfer was compounded of two components, β_H operating on the enthalpy of activation and β_s (as $T\beta_s$) on the $-T\Delta S^{\circ\ddagger}$ component of $\Delta G^{\circ\ddagger}$, for the overall activation process in the HER.

This situation regarding β and corresponding b values for steps I or II obviously introduces complications in the diagnostic assignment of b values to reaction mechanisms of the HER. A value of -118 mV for $T = 298$ K for a cathodic charge-transfer step with β being 0.5 is evidently fortuitous since b is rarely simply $2.3RT/(\beta = 0.5)F$!

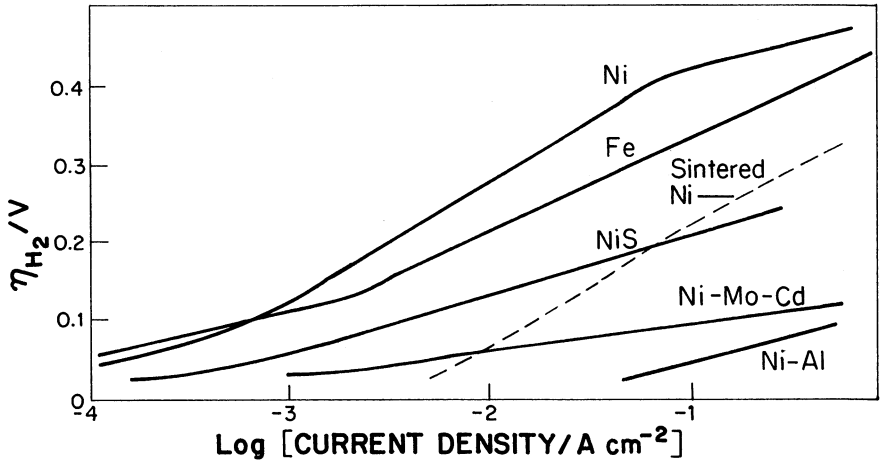

Fig. 5. Comparison of Tafel relations for the HER at various Ni electrode preparations and Fe, having varying real-to-apparent area ratios. $T = 343$ K (from Tilak et al. ref. [83], reproduced by permission of the publishers).

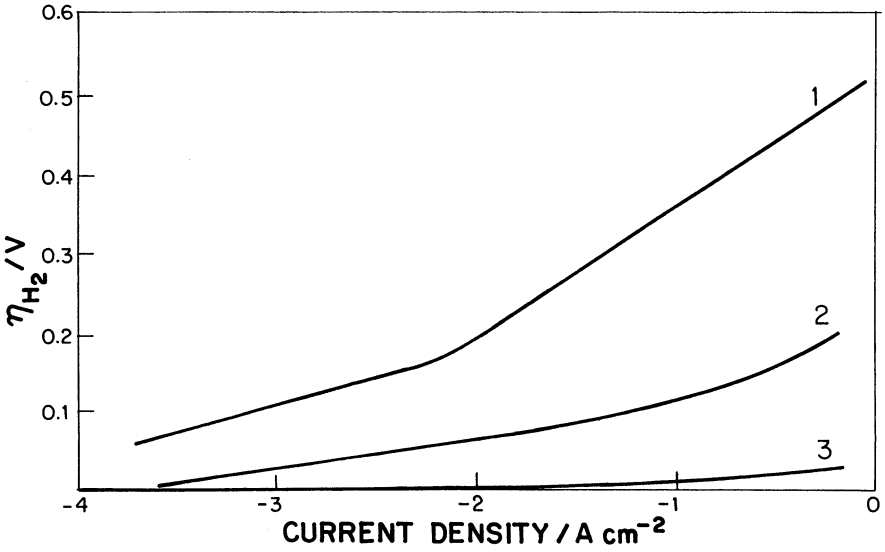

Fig. 6. Comparison of Tafel relations for the HER on three types of Pt: (1) smooth Pt; (2) high-area thermally formed Pt; and (3) Teflon-bonded Pt on Pt screen (from Tilak et al. ref. [83], reproduced with the permission of the publishers).

7. Experimental evaluation of surface coverage by H in the HER

7.1. Determinations of UPD and OPD H coverage

In relation to electrocatalysis and H electrosorption in the HER, information on coverage by the adsorbed (OPD) H intermediate (MH_{ads} in I, II and III in Section 6) in the HER is of major interest, especially with regard to its dependence on overpotential, η, and cathode metal, which determine the Tafel slope and exchange current-density of the HER.

In the case of the noble, H-adsorptive metals, coverage by UPD H is directly determinable by means of charging curves [7] or, more informatively, by cyclic voltammetry [8,11] or impedance spectroscopy [18] through evaluation of the potential-dependence of the H pseudocapaticance [33], arising prior to onset of cathodic H_2 evolution.

Experimental determination of coverage by OPD H, i.e. under conditions where continuous currents are passing for cathodic H_2 evolution at finite η values, cannot be conducted by recording of charging curves or cyclic voltammograms since the response currents for changes of OPD H coverage are usually very small and would be superimposed on substantially larger overall faradaic currents for cathodic H_2 evolution Information on OPD H coverage, therefore, requires use of a transient or modulation method and can be obtained as a $f(\eta)$ by means of two procedures: (a) recording and analysis of potential-relaxation transients following interruption of prior steady-state currents passing at various controlled η values; or (b) a.c. impedance spectroscopy [18,19] conducted at various η values for H_2 evolution.

7.2. Information from potential-relaxation transients

This procedure [57] was initiated by Conway, Bai and Tessier [58,59], based on recording and analysis of potential-relaxation transients following interruption of steady-state currents as in the method of Butler and Armstrong [60] for evaluation of double-layer capacitance at Hg. The full analysis of this procedure was given by Harrington and Conway [61], as illustrated in Fig. 7 showing how double-layer and pseudocapacitance charge relaxation can be distinguished in the time domain.

Essentially, this method gives information on the η-dependence of the OPD H pseudocapacitance, integration of which as $f(\eta)$ gives the potential-dependence of charge corresponding to changes of OPD H coverage with overpotential which determine, together with β, the Tafel slope (Eq. 8). Relaxation of the double-layer charge takes place in a short time-scale of μs–ms while that for the H pseudocapacitance arises over ten to 1000

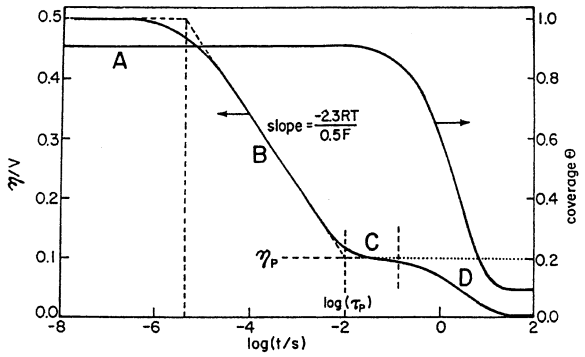

Fig. 7. Calculated potential–relaxation transients illustrating distinction between double-layer and adsorption pseudocapacitance charge relaxation in the time-domain. Regions A–B–C are for self-discharge of the double-layer capacitance component and C–D is that for any pseudocapacitance. Right-hand curve and scale are for time-dependence of coverage of an electroactive and scale are for time-dependence of coverage of an electroactive intermediate. e.g. adsorbed H, giving rise to the pseudocapacitance (from Harrington and Conway, ref. [61], reproduced with permission of the publishers).

times longer time-scales (cf. Fig. 7) and thus can be resolved from the double-layer response. Thus, this procedure leads to results in the time-domain analogous to those obtainable in the frequency domain using impedance spectroscopy (see Section 8.2 below).

Results are shown in Figs. 8 and 9 for H OPD capacitance and coverage as a function of η for the HER at three single-phase Ni–Mo alloy cathodes, data being derived from potential-relaxation transients [57]. The coverage values (Fig. 9) approach constant limiting values, <1, with increasing $-\eta$. This situation can only arise when step II is rate-controlling. If step III were rate-limiting, $\theta_{H,OPD}$ would increase continuously towards 1 as $-\eta$ was increased, corresponding to a b value initially of -0.029, increasing towards ∞, i.e. a non diffusion controlled limiting current for H+H recombination.

The behavior observed in Fig. 9 is accounted for as follows, in terms of kinetic equations for steps I and II of the HER as treated in Section 6. The respective kinetic equations in abbreviated form, i.e. including double-layer effects in the respective standard rate constants, are (with subscript numbers referring to respective reaction steps, I, II and III in Section 6.1)

$$i_{+1} = Fv_1 = Fk_1 c_{H^+}(1-\theta_{H,OPD})\exp\ -[\beta_1 F\eta/RT] \quad (9)$$

$$i_{-1} = Fv_{-1} = Fk_{-1}\theta_{H,OPD}\ \exp[(1-\beta_1)F\eta/RT] \quad (10)$$

and

$$i_2 = 2Fv_2 = 2Fk_2 c_{H^+}\theta_{H,OPD}\ \exp\ -[\beta_2 F\eta/RT] \quad (11)$$

$(i_1 - i_{-1}) = i_2$ in the steady-state and Eqs. (9), (10) and (11) can also include exponential terms of involving $\beta_2 g\theta_{H,OPD}$ (cf. [33]) if lateral interactions between H atoms across the surface are significant. Usually, it is

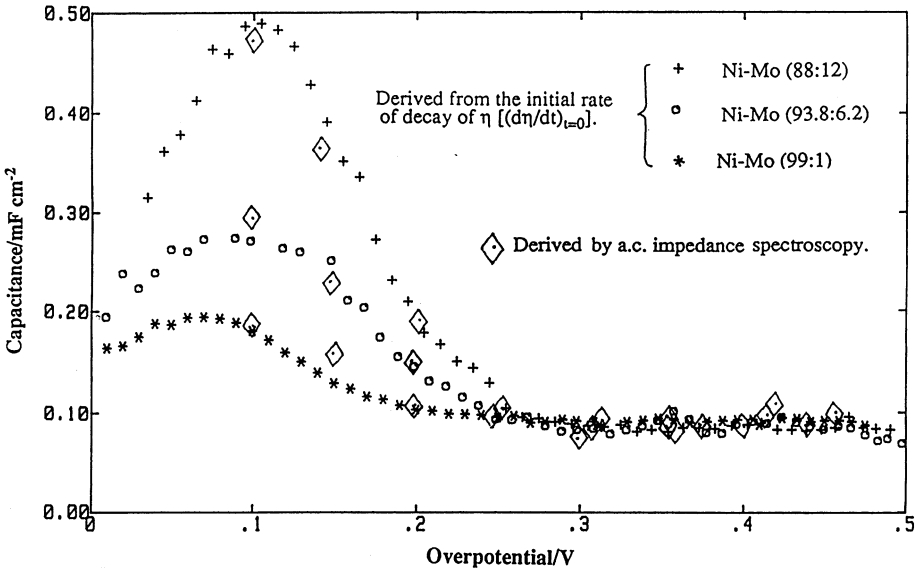

Fig. 8. OPD H adsorption pseudocapacitance profiles as a function of overpotential for three, single-phase Ni–Mo alloys, derived from potential–relaxation transients (from Conway and Brousseau, ref. [57]).

assumed that $\beta_1 \simeq \beta_2 = '\beta'$, though this may not necessarily be the case.

Abbreviating Eqs. (9), (10) and (11) respectively as $v_1 = l(1-\theta_{H,OPD})$, $v_{-1} = m\theta_{H,OPD}$ and $v_2 = n\theta_{H,OPD}$, say, for a given η, the steady-state condition for $\theta_{H,OPD}$, viz $d(\theta_{H,OPD})/dt = 0 = v_1 - v_{-1} - v_2$, gives

$$\theta_{H,OPD} = l/(l+m+n) \tag{12}$$

noting that l, m and n are exponential functions of η as in Eqs. (9), (10) and (11). Corresponding to Eq. (12), the H pseudocapaticance $C_\phi = q_1 d(\theta_{H,OPD})/d(-\eta)$

$$C_\phi = \frac{Fq_1}{RT}\frac{lm}{(l+m+n)^2} \tag{13}$$

with $\beta_1 \equiv \beta_2 = 0.5$, q_1 the charge equivalent to $\theta_{H,OPD} = 1$ and (for this example) ignoring possible interaction effects ($g \simeq 0$). Inserting the η-dependent factor and writing K_1 for k_1/k_{-1}, we obtain

$$\theta_{H,OPD} = 1/(1 + K_1^{-1} c_{H^+}^{-1} \exp[\eta F/RT] + k_2/d_1) \tag{14}$$

Then it is seen that, at sufficiently large cathodic overpotentials, $\theta_{H,OPD}$ can reach limiting values for the mechanism I, II, given by

$$\theta_{H,OPD}(\lim) = 1/(1 + k_2/k_1) \tag{15}$$

so that attained limiting coverages depend on k_2/k_1, while $\theta_{H,OPD} \to 1$ as $k_2/k_1 \ll 1$. Thus, Eq. 15 represents the type of experimental behavior found in Fig. 9.

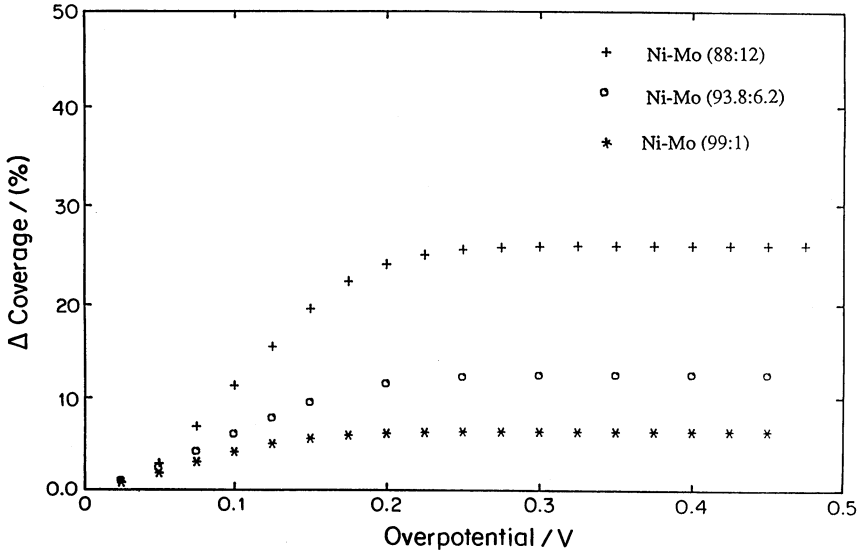

Fig. 9. OPD H coverages during the HER at the three Ni–Mo alloys of Fig. 8 derived by integration of the pseudocapacitance profiles of Fig. 8 (from Conway and Brousseau, ref. [57]).

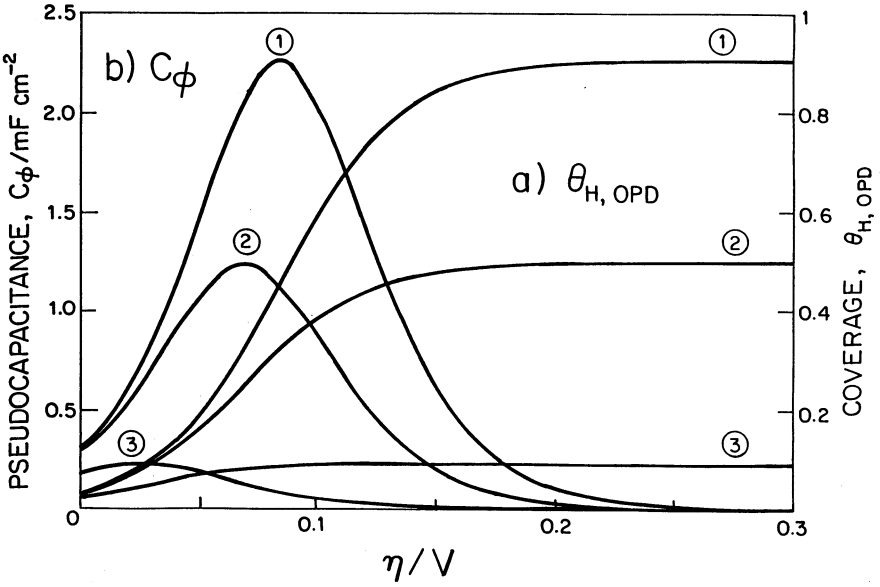

Fig. 10. Calculated plots of OPD H pseudocapacitance and integrated H coverage values according to Eqs. 13 and 14, respectively; compare with experimental curves in Fig. 8 and Fig. 9.

Calculated plots of $\theta_{H,OPD}$ versus η for three k_2/k_1 values, using Eq. (12) and the corresponding C_ϕ versus overpotential plots using Eq. (13), taking $c_{H^+} = 1$, $q_1 = 257\ \mu C\ cm^{-1}$ (for H at Ni) and $T = 298$ K, are shown in Fig. 10. Limiting coverages, $\theta_{H,OPD}$ (lim), arise for the above reaction mechanism, depending on various k_2/k_1 ratios (Eq. (15), as seen in the plots of Fig. 10.

When a desorption step is rate-controlling, an alternative assumption is often made that step I is in quasi-equilibrium (k_1, $k_{-1} \ll k_2$ or k_3 [for recombination control]), so that $\theta_{H,OPD}$ becomes directly expressible, in the well known quasi-thermodynamic way [33], from

$$\frac{\theta_{H,OPD}}{1-\theta_{H,OPD}} = \frac{k_1}{k_{-1}}\, c_{H^+} \exp\, -[\eta F/RT] \qquad (16)$$

which is formally similar to the equation for UPD H but with the exp factor involving a negative η for H_2 evolution. In the case of the Tafel desorption pathway III, involving recombination of OPD H atoms at finite (negative) η (see Section 8 later) the same quasi-equilibrium expression [Eq. 16] for $\theta_{H,OPD}$ applies if $k_3 \ll k_1, k_{-1}$ but $> k_2$ However, the steady-state expression does not lead to a simple relation for $\theta_{H,OPD}$ as $f(\eta)$ due to the quadratic form of the rate equation in $\theta^2_{H,OPD}$, as is well known.

7.3. Spectroscopic identification of adsorbed H at electrodes

Characterization of the state of chemisorption of H at electrode metals by IR-spectroscopy is rendered difficult by the ubiquitous presence of solvent water having –OH stretching frequencies in the same range as those expected for metal-to-H (MH) at e.g. Pt surfaces in the infra-red. In fact, any stretching vibration of H to an appreciably heavier atom will have a frequency on the order of 3300–3500 cm^{-1} on account of the reduced atomic mass of H in its bond being close to 1. Possible coupling by H-bonding to adsorbed water at the electrode interface is a likely complication [13,20].

However, in potential-modulated IR-spectroscopic studies of the Pt surface near the H_2 reversible potential, Bewick et al. [62–65] have claimed to be able to detect responses associated with electrosorbed H, H-bonded to water [66]. Potential modulation at Pt near the reversible potential, gives rise to water-like IR-absorption bonds only over the potential range of +0.06 to +0.18 V, RHE, where the weakly-bound state of UPD H arises. The bonds observed all have the same sign in the differential absorption experiment and correspond to increased absorption when the weakly-bound H is formed. A complication is, however, involved in that it is that potential range (at Pt) when desorption of HSO_4^- ion (in aq. H_2SO_4 electrolytes) is becoming significant. The IR-absorption behavior was, however, found, in general, to be relatively insensitive, in the wave-length range 1.7–2.2 μm, to the type of anion present: HSO_4^- or SO_4^{2-} in aq. H_2SO_4, ClO_4^- in aq. $HClO_4$ and Cl^- in 1 aq. $HClO_4 + 2.5 \times 10^{-3}$ M HCl. This is surprising result since cyclic voltammograms for Pt in the UPD H range of potentials are quite sensitive to the type of co-anion present. A puzzling result is that bonds for adsorbed H_2O are not observed at potentials more positive than 0.18 V where the strongly bound UPD H component begins to arise at polycrystalline Pt. This could be due to the H being bound in hollow coordination sites on Pt where the H is protonic (cf. [41]). Possible structures for the H-bonding interaction between chemisorbed H and

co-adsorbed water molecules were considered but the mean OH dipole orientation is potential dependent [67].

Later work by Bewick with Nichol [65,66], on H absorption at polycrystalline Pt, Rh and Ir, and Pt(111) in aq. H_2SO_4 up to 1 M concentration confirmed the possibility of identifying a chemisorbed state of H in the HER. At the potential for onset of the process, an IR-adsorption band arose at 2090 cm^{-1} which was assigned to atop H-metal vibration, also based on potential-dependence of the bond-frequency. However, some questions have been raised [68–70] whether this bond is really associated with UPD or OPD H, with the conclusion that UPD-type H is not in the same state as the OPD intermediate in the HER. As noted in [80] and Section 5, the matter is thermodynamically ambiguous, depending on the fugacity of H_2. Notwithstanding such doubts, Ogasawara and Ito [71] have indicated that an atop H state can also be observed at Pt(100), Pt(110) and Pt(111)–[6(100) × (111)]. Continuing confirmation of IR-spectroscopic identification of atop UPD H, within +0.1 V of the onset of the HER at Pt in high-purity 0.1 M H_2SO_4 was found by Nanbu et al. [72]. A band arises between 2030 and 2070 cm^{-1} due to OPD H and was distinguishable from a band at 2010 assignable to adsorbed CO arising from reduction of traces of CO_2. Over a wider range of potential where H_2 was forming, the atop H-to-metal bond was said to be unequivocally observable.

This work appears to offer definite support for the spectroscopic observability of both UPD and OPD H, depending on the electrode potential relative to the HER reversible potential. The atop H state can be concluded to be the adsorbed intermediate in the HER at finite overpotentials while the UPD H is similarly identifiable over a narrow UPD potential range. There is a small frequency difference of the band maxima for atop H observed in UPD and OPD potential ranges but this is probably due to lateral interactions and/or anion co-adsorption effects; geometrically, the coordination of H seems to be the same, viz. an atop configuration.

8. H chemisorption and surface specificity in the kinetics and mechanism of the HER

8.1. Data representation and experimental requirements

The mechanism(s) and kinetics of the HER have been treated in the literature in a large number of papers for a variety of cathode metals. The kinetic data are usually represented by values of the constants a and b of the Tafel equation "$\eta = a + b \log j$", where η is the overpotential and j the current-density for equilibrium at $\eta = 0$.

Until relatively recent years, a, b and $\log j_0$ values for the HER at various metals have been discrepant. This has been due to: (a) inadequate purity of solutions (note traces of heavy metals can be readily deposited in HER experiments and materially change the surface composition of cathodes—a submonolayer can be sufficient!); (b) differences of surface preparation of cathodes (except Hg or Ga); and (c) a third point, often of practical significance as it determines true j_0 values, is the real-to-apparent area ratio or the roughness factor of the electrode surface. This factor is important when comparing electrocatalytic activities for the HER of various electrode preparations, e.g. porous electrodes such as Ni–Mo composites [35,57] or alloys of transition metals [43,72]. In some publications, this essential normalization factor has not always been applied, so the real-area factor can overwhelm any intrinsic differences of electrocatalytic activity due to band-structure in alloying [72,73], etc.

The works of the Frumkin school in Russia established some of the first reliable data for Hg and Ni while Azzam, Bockris, Conway and Rosenberg [74] examined quantitatively the basis of 'pre-electrolysis' of solutions for obtaining high purity conditions. The novel technique of one of the present authors (BEC) for sealing metal wires into thin glass bulbs in pure H_2 gas at approximately 600–700 °C, enabled clean and reproducible solid-metal surfaces to be generated, and protected until used in the cell.

The use of 'pyrodistilled' water for high-purity experiments was initiated by Conway et al. [75] while later the satisfactory use of 'Milli Q' distilled water was demonstrated in works by Hamelin and Clavilier at CNRS, Meudon, and established a new high standard for pure water production. General requirements for high-purity, electrode–kinetic measurements, especially for the HER and H chemisorption, were reviewed by Angerstein-Kozlowska [76].

The availability of reliable and reproducible electrode-kinetic data is of major importance for establishing and interpreting dependence of mechanisms of the HER on the types and properties of cathode metals (see below). A critical examination of $\ln j_o$ and H-to-metal bond energy values was given by Trasatti [77] and earlier by Conway [78] for $\ln j_o$.

8.2. Information from impedance spectroscopy

In a complementary way to the time-domain method in Section 7.2, similar and fuller information on H coverage behavior in the HER in relation to the latter's kinetics at controlled potentials can be obtained by impedance spectroscopy. This was first applied by Frumkin, Dolin and Ershler [79] to Pt, later by Breiter [81] and more recently by Barber, Morin and Conway [18,81] to studies of OPD H at single-crystal Pt surfaces (note that on such Pt surfaces, the states of UPD H up to the H_2 reversible potential had been thoroughly

studied earlier by Clavilier et al. [11], and by Jerkiewicz et al. [30] with respect to temperature effects on UPD H states).

In the impedance approach, the frequency-dependence of the real (Z') and imaginary ($-Z''$) components of the reaction's impedance behaviour are measured and usually plotted in the complex-plane against each other in a so-called Nyquist plot, together with the frequency dependence of the phase angle, ϕ. The observed behaviour is usually fitted to an equivalent circuit resistive and capacitative components representing the double-layer capacitance, C_{dl}, Faradaic resistance, R_F, H adsorption pseudocapacitance, C_ϕ, and a Warburg element, W, representing diffusional impedance are usually included.

In the HER at clean, active Pt, single crystals and Pt(poly) the Tafel relations are found, e.g. in the work of Breiter [80], to be influenced by diffusion. However, this is not usually diffusion of the reacting H_3O^+ ion (in acid) to the Pt surface but diffusion of H_2 out from a supersaturated H_2-lamina in the diffusion layer. This can set up a local pseudo-reversible potential leading to an apparent Tafel slope of approximately -29 mV per decade which can be confused with the consequence of rate-controlling H+H recombination (Tafel's step III), probably dependent on OPD H coverage.

Barber et al. [18,81,82], in their impedance studies at Pt (*hkl*) electrodes, also conducted electrode-rotation experiments in order to avoid the H_2 diffusion effect. However, they found the order of kinetic activity of three Pt surfaces for the HER in 0.5 M H_2SO_4 to be (100 S_{II}) < (111) < (110) (Fig. 11), measured at 2500 rpm over a current-density range 10^{-3}–4×10^{-1} A cm^{-2}, corresponding to an η range of -0.01 to -0.18 V, also a short range. The difference in order of the activities from those of Markovic et al. [39,40] could be due to the difference of pH and electrolyte anion, especially as both sets of data are for potentials quite near the reversible potential.

In a detailed impedance spectroscopy study of the HER at Pt(111), (110) and (100) surfaces in 0.5 M NaOH, Barber and Conway [74] analysed the frequency response over the range 50 kHz–0.5 Hz in terms of the Faradaic admittance, y_f, and the total impedance, Z_{tot}, where

$$Y_f = A + B/(i\omega + C) \quad (17)$$

and

$$Z_{tot} = R_s + (y_f + i\omega C_{dl})^{-1} \quad (18)$$

Parameters A, B and C are obtained as derivatives of quantities in the kinetic equations ([81]) for the respective reaction steps I, II and III in the HER.

Fig. 11 shows how the complex-plane plots depend appreciably on the index of the Pt crystal face while Fig. 12 shows the marked dependence of the A parameter of

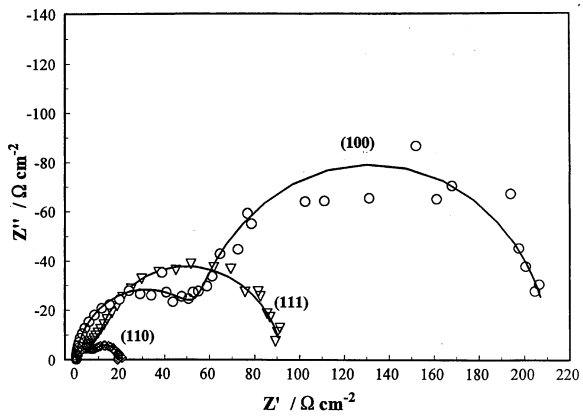

Fig. 11. Complex-plane impedance plots for the HER at Pt (*hkl*) surfaces in 0.5 M aq. H_2SO_4 showing sensitivity to 2-d surface structure (from Barber and Conway, ref. [81], and ref. [18], reproduced by permission of the publishers).

Eq. 17 $-F(dr_o/d\eta)$, on crystal face (r_o = flux of electrons at the Pt surface). The y_f data were determined at an electrode rotation rate (hanging meniscus) of 3000–4000 rpm beyond which no further change of the complex-plane plots arose. Note that in 0.5 M H_2SO_4, frequency–response behaviour was obtainable only at the (111), (110), (511) and (100) s_{II} faces; at other faces (in acid) the kinetic relaxation frequencies are too high for satisfactory responses to be recorded. The order of reactivity increases from (100) s_{II} to (110), parallel to the increasing dominance of the H_2 diffusion effect. Details must be followed in the cited papers.

8.3. Information from rotated electrode studies on the HER

For some time it has been realized that diffusion processes involving cathodically produced H_2 can dominate the kinetic measurements of the HER because clean Pt electrodes are highly active for the process, so that dependence of the kinetics on surface geometry of

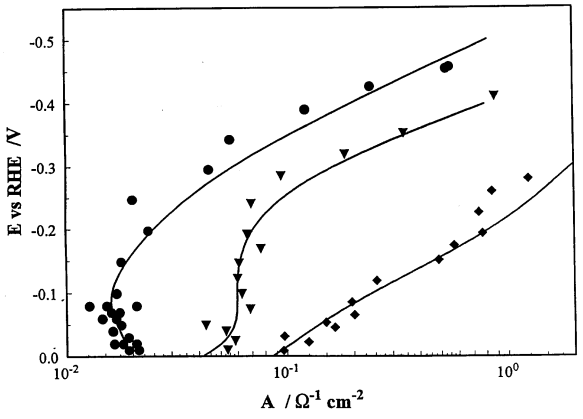

Fig. 12. Showing marked dependence of the admittance parameter A of Eq. 17 for the HER at Pt (*hkl*) surfaces in aq. 0.5 M H_2SO_4 (from Barber and Conway, ref. [81] and ref. [18], as for Fig. 11).

single-crystal electrodes can be obscured by the diffusion effect. This has led to the incorrect impression (see below) that the kinetics of the HER are insensitive to surface structure, e.g. at Pt.

This complicating situation can be dealt with in impedance and in d.c. current–voltage curves by high-speed rotation of the electrode, as in refs. [39,40], and in the impedance analysis by treating the data in terms of a 'finite diffusion' model [17,18,81] and the Warburg impedance referred to above.

Studies on hydrogen electrochemistry (the HER and the HOR) were conducted by Markovic et al. [39] in alkaline solution at Pt low-index single-crystal surfaces, (111), (100) and (110). On the cathodic, HER side, only a small but significant dependence of H_2 evolution current-densities on electrode rotation rate (ω) was observable on all three single-crystal faces, indicating a role of H_2 diffusion from a supersaturated boundary layer. However, at $\omega = 3000$ rpm, or higher, the H_2 supersaturation effect became eliminated. The polarization curves for H_2 evolution (and oxidation) shown in Fig. 13 indicate (but only over a short $-\eta$ range of ca. 0.05–0.21 V, RHE) that the kinetic activity for the HER at Pt (*hkl*) increases in the order $(111) \ll (100) < (110)$.

Similar experiments conducted in 0.05 M H_2SO_4 at the three Pt single-crystal surfaces gave exchange current-densities for the HER/HOR which increased in the order $(100) \ll (100) < (110)$ with the j_o for Pt (110) being 3 × that at the (111) surface, i.e. the same order as that for alkaline solution [39]. Comparisons between the (micro-) polarization lines for the HER and HOR on the three surfaces are shown in Fig. 14. Note that the order of activities for the HOR is the same as those for the HER, as potentials pass across the reversible value (Fig. 14), as may be expected in the micro-polarization regions. Fig. 15 shows current versus potential relations for the HOR at several single-crystal Pt surfaces for various electrode-rotation rates. Significant structure sensitivity is observed [39].

Interestingly, it was concluded [39,83] that the strongly-bound state of H is not involved in the HER which is consistent with the factors determining positions of metals on the electrocatalysis 'volcano curve' for $\log j_o$ versus MH bond energy (see Fig. 17 in Section 9). This is in agreement with the view of Conway and Jerkiewicz [83] that it is the OPD state of H that is involved in, and determines the kinetics (hence j_o) of the HER. Related to this matter is the conclusion of Markovic et al. [39] that for all Pt surfaces to provide an appreciable rate of the HER, some of the UPD H has to be in a sub-surface state (e.g. coordinated in hollow sites, cf. Horiuti and Toya [41], in order to provide pairs of 'bare' Pt sites which can be occupied by the kinetically significant (cf. [83]) OPH H intermediate. Note that further detailed arguments are given in [39,40] and in [13], concerning the states of adsorbed H in relation to the HER but space limitation here prevents further discussion.

In experiments at single-crystal Pt surfaces over a range of temperatures [40], Markovic et al. found that structure-sensitivity of the HER kinetics was substantially greater at low temperatures (274–298 K) than at higher ones (333 K). This could be due to diminished 2-d mobility of H at the lower temperatures associated with the entropy of adsorbed H (cf. [28,30]) or simply by slowing down the otherwise rapid kinetics of the HER which are otherwise obscured by the H_2-diffusion effect [14,40].

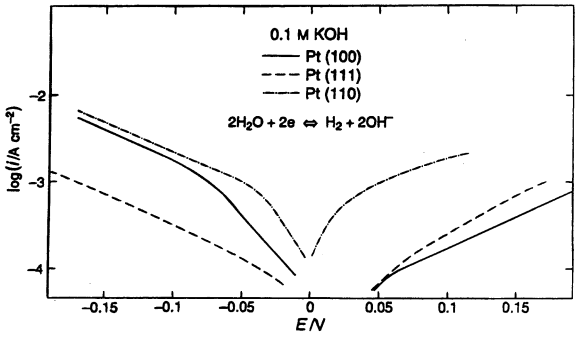

Fig. 13. Anodic (HOR) and cathodic (HER) polarization curves for the indicated Pt(*hkl*) surfaces (from Markovic et al. Ref. [39], reproduced with permission of the publishers).

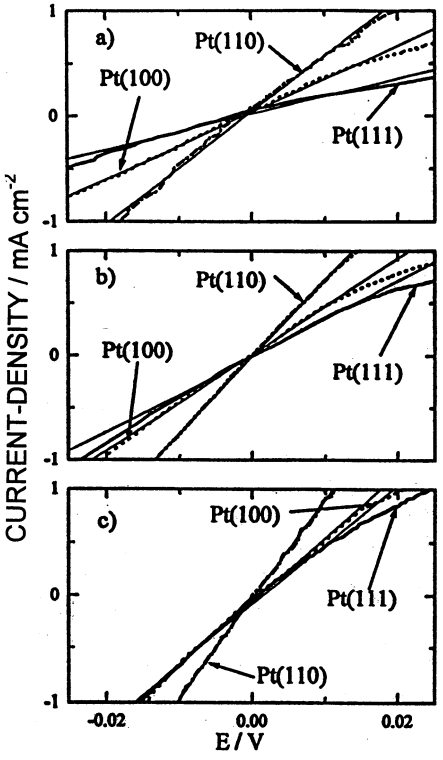

Fig. 14. Micropolarization lines for the HER and HOR around the reversible potential for three surface orientations of Pt electrodes (from Markovic et al. ref. [39], reproduced by permission of the publishers).

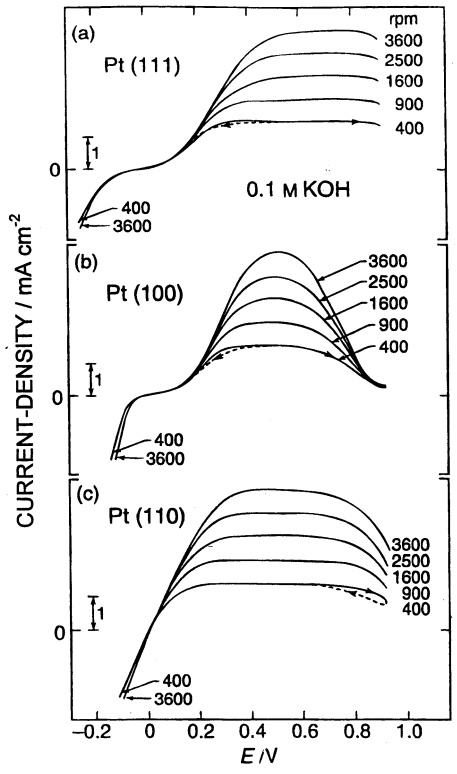

Fig. 15. Plots of current vs. potential relations for the HOR at several single-crystal electrode surfaces for various electrode rotation rates (from ref. [39], reproduced by permission of the publishers).

In the HOR direction, beyond +0.05 V, the reaction rates are determined by mixed kinetic/diffusion control at low anodic potentials while above +0.05 V well defined diffusion-influenced currents arise [39,40], with j being proportional to $\omega^{1/2}$ (see Fig. 15). Comparative Tafel plots for the HER and OER at the three Pt surfaces in 0.1 M KOH at $\omega = 3600$ rpm are shown in Fig. 16; however, although the plots cover only a short range of polarization potentials around zero V, RHE, they do demonstrate sensitivity of the HER and HOR kinetics to the Pt surface geometry, as in Fig. 13.

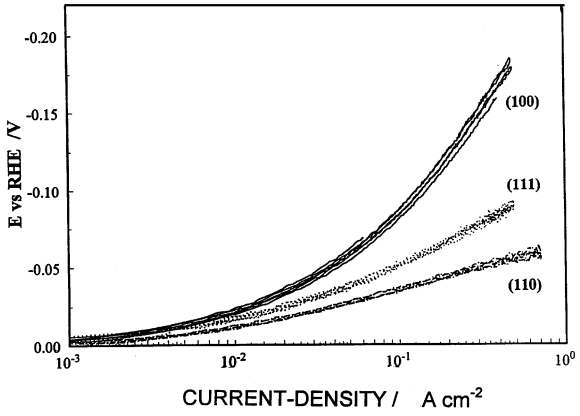

Fig. 16. Polarization curves for the HER and HOR on Pt(*hkl*) in 0.1 M KOH at 3600 rpm.

9. HER kinetics and their relation to cathode metal properties

9.1. Phenomenology and experimental data

In relation to mechanisms of the HER and $\log j_o$ values, extensive interest has arisen in the dependence of $\log j_o$ for the HER on properties of the substrate cathode metal, e.g. electron work function Φ and energy of chemisorption of H. A clear, apparent, dependence of $\log j_o$ values on Φ was demonstrated by Bockris [44] for a series of metals in two families: Tl, Pb and Hg, low $\log j_o$; and a variety of sp and d metals having much higher $\log j_o$ values. However, these relations to Φ [13,84] cannot be primary since Φ always cancels out around any real circuit for electrode-kinetic measurements as a function of overvoltage, as pointed out later (1957) in work by Conway and Bockris [85]. The relations must be plotted in terms of metal-to-H bond energy [77] which, being itself dependent on Φ [85], accounts for the actual apparent dependence of $\log j_o$ on Φ.

Using later and better data for $\log j_o$ and for chemisorption energies of H, Trasatti [77] demonstrated a clear relation between these quantities having the form of a 'volcano' curve (Fig. 17) as has been found in the field of regular gas/solid heterogeneous catalysis.

The existence of a volcano plot for HER kinetics in alkaline solutions is less well founded than for acidic solution: (a) because much less comparative data are available and (b) because such data as do exist are less reliable and older, the former because 'clean' electrode-kinetic experimentation is more difficult to conduct and may also be affected by ingress of CO_2 leading to formation of CO_3^{2-} anions, except in $Ba(OH)_2$ alkaline electrolyte (but rarely used). A significant and additional point, emphasised by Petrii and Tserlina [86], is that the rate-controlling step for the HER in alkaline solution can be different, e.g. for Ni [87,88], from that in acidic solutions where j_o values are usually larger by an order of magnitude or less (see [89]). The origin of this difference is attributed to the different identities of the proton sources, H_3O^+ or H_2O, in acid or alkaline solutions, respectively.

9.2. Theoretical aspects of volcano plots

Originating from the relations treated by Bockris [13], and by Conway and Bockris [44], Parsons [89] gave a fundamental treatment of the origin of the volcano relation for the $\log j_o$ values but as a function of the standard Gibbs energy, ΔG°_H, of chemisorption of 2H from H_2 at equilibrium. The volcano relation arises essentially because $\log j_o$ for various mechanisms of the HER can be expressed [89] in terms of the product $(\theta_H)^\beta (1-\theta)^{1-\beta}$ as a function of ΔG°_H which has a maximum

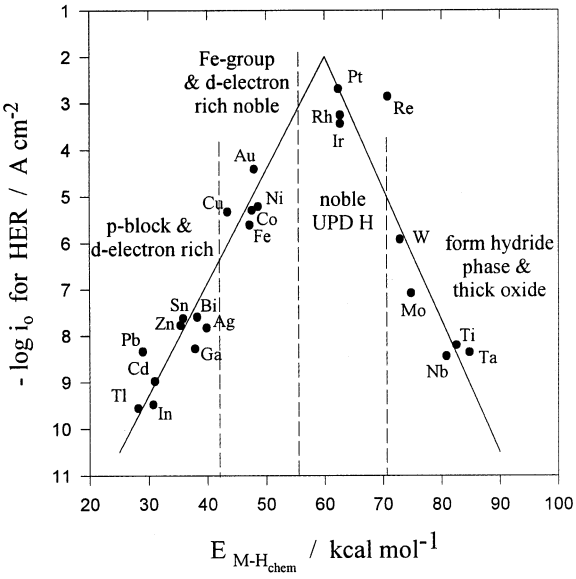

Fig. 17. Volcano curve for electrocatalysis of the HER at various metals in terms of dependence of log j_o values on metal-to-H bond energy (from Trasatti, ref. [77], with editorial modifications as in ref. [31]).

when [78] $\theta_H = 1-\theta_H = 0.5$ $(\beta = 1-\beta)$ corresponding to $\Delta G^\circ_H = 0$. This treatment is to be regarded as one of major importance in electrocatalysis.

In the light of the discussion above, one of the important conclusions [38] is that the kinetically significant adsorbed (OPD) intermediate in the HER at Pt and related metals is not the strongly bound UPD-type of H but, rather, the extra, weakly bound OPD H which is deposited on, or with, the pre-existing UPD H layer. This, then, is what determines the location of the Pt group metals on the volcano plot [77,89] as the most kinetically active for the HER. Parsons had noted an analogous point in his 1958 paper [89], viz that charging curves indicate appreciable (UPD) H coverage at Pt so that, on the basis of Temkin adsorption behaviour, his g° could approach zero. However, the distinction between UPD and OPD of H was not, at that time, addressed or well understood.

We have remarked that Markovic et al. [39] have concluded that the UPD H layer at Pt functions as an inhibitor of the kinetics of the HER. Our analysis [83] corresponds to an opposite conclusion; because of the supposed weaker binding of the OPD H compared with that of the UPD H, the kinetically relevant ΔG°_H, i.e. $\Delta G^\circ_{H,OPD}$, is brought nearer to the theoretically significant $\Delta G^\circ_H = 0$ condition (or g° of [89]) so that the Pt metals then do actually lie at or near the apex of the volcano plot [77] instead of on its right-hand branch (Fig. 18), if the ΔG°_H for UPD H were to be plotted.

The conclusion then is that the HER proceeds with high j_o at the 'Pt metals' because it takes place on an hydrided surface via OPD H rather than at bare metal for which the bonding energy to H would be much larger than that at the UPD H-coverage surface, as illustrated in Fig. 18.

Comparative evaluations of intrinsic electrocatalytic activities of metals and alloys have often been made in the basis of relative values of log j_o for the HER [77,85,89,90] especially for alloys of the Brewer type by Jaksic [90]. However, for practical purposes, the comparative values of the Tafel slope, b, are also of importance, at least equal to that of log j_o values. Thus, some metals that have relatively poor j_o values can have low Tafel (b) slopes, so that their performance in terms of overvoltage at practical current-densities (say 1 A cm^{-2}) can be quite favorable [90]. The essence of this point is that comparisons based on log j_o values alone give only a measure of kinetics at the equilibrium or zero-polarization condition while comparisons on the basis of b values [91] (as well as log j_o, cf. [85,89]) provide a complementary mechanistic aspect of the kinetic behaviour under practical operating conditions. These matters are of importance for optimization of operation and performance of electrolysers for H_2 production and, e.g. for selection of cathode materials for the chlor–alkali process [45].

10. Electrocatalysis in the HOR

10.1. Molecular level processes in the HOR

The elementary steps in the HOR are the reverse of those, I, II or III, considered earlier for the HER. However, diffusion of the H_2 reagent is commonly rate-limiting but can be mediated by high-speed electrode rotation [39] or use of porous 'gas-diffusion' electrodes. The diffusion effects lead to difficulties in obtaining well characterized Tafel slopes for the HOR at various anodes.

When the HOR is proceeding, the potential is, 'by definition', positive to the RHE potential so the state of the intermediate resulting from dissociative adsorption of H_2 should be that of UPD H, resulting from the reverse of processes II and III (Section 6.1): in one case the adsorbed H results from dissociative ionization (reverse of step II) or, in the other, from regular dissociative chemisorption (reverse of step III). These are the key processes in fuel-cell oxidation of H_2, although they can be rate-limited by diffusion since the solubility of H_2 is small and diminished by 'salting-out' in the strong electrolyte solutions normally used.

Once the dissociative adsorption has taken place, the anodic oxidation of the UPD-type H can be rapid, corresponding to the known high j_o value (derived from the large s_o observed [92] in cyclic voltammetry over the UPD H region). The same situation arises in the anodic oxidation of H diffused through Pd in an H-transfer

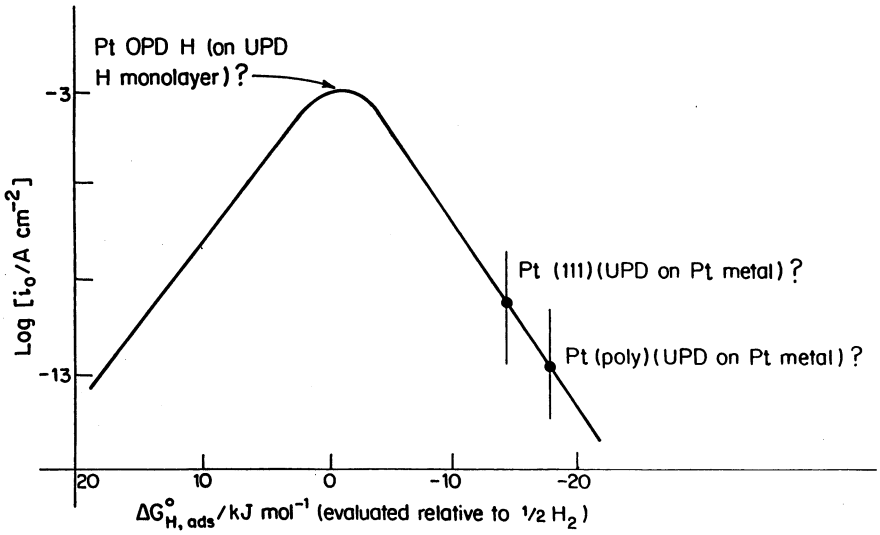

Fig. 18. Location of Pt on the volcano curve of Fig. 17 if the UPD H bond energy were plotted for the strongly-bound H species in relation to a supposed OPD H bonding (from Conway and Jerkiewicz, ref. [31]. Reproduced with permission of the publishers).

experiment: the diffused H is rapidly desorbed as H^+ (or H_2O) at the anodic transfer interface. Additionally, it has been shown [93] that H, underpotentially deposited at Pd, becomes transferred by diffusion and oxidized rapidly at the exit side of a Pd membrane.

Therefore, apart from slowness of diffusion of H_2 in solution, the electrode-kinetics of H_2 oxidation are determined by one or other of the H_2 dissociation processes. This is the real electrocatalytic step in the HOR and hence in fuel-cell oxidation of H_2.

10.2. Results of experimental studies on the HOR

First we note that HOR studies were already discussed in Section 8 in the context of its relation to HER kinetics and results at single-crystal surfaces in the work of Markovic et al. on the HER/HOR.

Results of kinetic studies on smooth noble metal surfaces in acidic and alkaline media are presented in Tables 1 and 2, along with the kinetic data for other materials [94–99]. These investigations reveal platinum to the most active among the noble metals in acid solutions, the slow-step being the dissociative adsorption of H_2. Since the HOR is a fast reaction at Pt, diffusion-control arises already at low potentials, necessitating the use of rotating electrodes or high surface area electrode structures for determining the kinetic parameters.

It is well known, as noted above, that electrolytic oxidation of dissolved H_2 gas is complicated by diffusional effects associated with its low solubility, approximately 10^{-3} mol l^{-1}. Commonly, this problem is attenuated by employing high-speed, rotating disc electrodes. A different approach was, however, taken in work by Bagotzki and Osetrova [100], using a Pt micro-electrode held just in the thin electrolytic film above the solution meniscus. This enabled H_2 oxidation kinetic behaviour to be followed up to diffusion-limited current-densities some ten times greater than those accessible at rotating-disc electrodes. In particular, current versus potential curves were able to be studied as a function of pH from 3.0 to 12.2 enabling the pH-dependence of true H_2 oxidation exchange current-densities, $\log j_o$, to be evaluated between pH 1.6 and 14. Notably, $\log j_o$ values fall from $+0.4$ (at pH 1.6) to -1.05 at pH $\simeq 3.5$, followed by independence of $\log j_o$ on pH between pH 3.5 and 14 suggesting [87,88] that the kinetic of H_2 oxidation proceeds by two alternate mechanisms: one depending on coverage (θ_H) by H (dissociated from H_2) and the other not depending on θ_H, i.e. an electron-transfer step prior to dissociation. Alternatively, the lack of pH-dependence of $\log j_o$ above pH 3.5 implies a role of OH^- ion in the rate-controlling step instead of H_3O^+ at pH < 3.5, viz the reverse of the so-called 'electrochemical mechanism' of the HER: $OH^- + H_2 + M \rightarrow MH_{ads} + H_2O + e$ compared with $H_2 + M + H_2O \rightarrow MH_{ads} + H_3O^+ + e$ (low pH), but this is argueable.

Ross and Stonehart [101], and Vogel et al. [96], confirmed the slow-step in the HOR as being dissociative adsorption of H_2 on smooth Pt, Pt-black and Pt supported on carbon in hot 96%H_3PO_4, and found that platinum crystallite size, down to 3 nm, has no effect on either j_o or b. They ruled out H spill-over from Pt to C on the Pt/C electrodes influencing the rate of the HOR. Urrisson et al. [102], on the other hand, observed a 4-fold increase in j_o as the platinum surface area was varied from 26 to 51 m^2 g^{-1} and found 1.5–2 orders of

Table 1
Kinetic data for the HOR in acid media

Metal/substrate	Medium (temperature in °C)	Tafel slope (mV)	Exchange current-density (mA cm^{-2})	Reference
Smoth Pt	0.5 N H_2SO_4 (22)	30	1.9	[84]
	1 N H_2SO_4 (25)	32	1	[85]
	96% H_3PO_4 (22)	30	27	[86]
Pt black (27 m^2 g^{-1})	96% H_3 PO_4 (22)		21	[86]
Pt on carbon (80 m^2 g^{-1}: Pt:1 mg cm^{-2}	96% H_3PO_4 (22)		18	[86]
Pt–Polyaniline: Pt loading (μ cm^{-2})	96% H_3PO_4 (22)			[87]
5		62	0.025	[87]
47		39	0.52	[87]
100		41	1.4	[87]
166		36	1.8	[87]
327		34	1.9	[87]
Bulk Pt+polyaniline electrode		43	1.5	
Smooth Ir	1 N H_2SO_4 (25)	50	0.398	[85]
Smooth Rh	1 N H_2SO_4 (25)	38	0.298	[85]
Smooth Pd	1 N H_2SO_4 (25)	100	1.28	[85]
Smoth Au	1 N H_2SO_4 (25)	105	0.007	[85]
MnP_3	1 N H_2SO_4 (22)		10^{-5}	[88]
FeP_3	1 N H_2SO_4 (22)		0.035	[88]
CoP_3	1 N H_2SO_4 (22)		0.05	[88]
NiP_3	1 N H_2SO_4 (22)		0.015	[85]

magnitude differences in apparent j_o between smooth and highly dispersed Pt (180 m^2 g^{-1}) supported on carbon. Pretreatment of Pt electrodes was also found to influence the catalytic activity for the HOR. Thus, it was reported [103] that the activity of annealed Pt was less than at electrodeposited Pt. This was attributed to the rearrangement of metastable Pt surface atoms to stable lattice sites by annealing, compared with regeneration of stable Pt atoms by the electrodeposition route. However, the real specific areas may have differed. These results are contradictory to the observations of Osetrova and Bagotskii [104], who noted a decrease in the j_o for the case of electrodeposited Pt. Oxidized Pt electrodes were reported to be covered by O species on 10% of the active sites with the HOR taking place on less active sites [105].

Mello and Ticianeli [106], examined the HOR on smooth Pt and Pt/polymer (Nafion) interfaces in x M $H_2SO_4+(1-x)$ M K_2SO_4 mixtures in the pH range 0.2–7.5 and found the Tafel slopes to be −33 to −37 mV up to an x value of 0.05, and ~42 mV at $x=0$ and 5×10^{-5} M. Dissociative chemisorption of H_2 was suggested as the rds in acid solutions and dissociative ionization as the rds in near-neutral solutions.

Pt-modified polyaniline electrodes, with varying loadings of Pt, were investigated in 0.5 M H_vSO_4 at 20 °C [97] and exhibited progressively decreasing Tafel slopes, from a value of −62 to −34 mV, as the Pt loading increased from 5 to 166 μg cm^{-2}. When the Pt loading was further increased to 327 μg cm^{-2}, the Tafel b and j_o values were found to become identical with those observed at bulk Pt electrodes. The b value of −40 to −50 mV was attributed to slow dissociative ionization

Table 2
Kinetic data for the HOR in alkaline media

Metal	Medium (temperature in °C)	Tafel slope (mV)	Exchange current-density (μA cm^2)	Reference
Pt	0.1 N NaOH (25)	105	398	[85]
Rh	0.1 N NaOH (25)	120	100	[85]
Pd	0.1 N NaOH (25)	105	250	[85]
Au	0.1 N NaOH (25)	125	1.28	[85]
Fe	0.25 N NaOH (25)	60	~100	[85]
Ni	0.1–1 N NaOH (25)	25	1	[85]
Raney Ni	6 M KOH (22)		0.45	[89]
Raney Ni+2% Ti	6 M KOH (22)		1.75	[89]
Raney Ni+7% Mo	6 M KOH (22)		5.4	[89]
Raney Ni+21.3% Mo	6 M KOH (22)		9.1	[89]

and −30 to −40 mV to the slow dissociative adsorption of H_2. It was shown that the progressive filling of the polyaniline matrix by spherical particles of Pt of constant diameter ~130 nm, could account for the j_o-dependence on the Pt loading. Mukerjee and McBreen [107] evaluated the influence of alloying using carbon-supported Pt, PtMn, PtCr, PtFe, PtCo and PtNi alloys at a Pt loading of 0.3 mg cm^{-2} at 95 °C and 5 atm pressure in 1 M $HClO_4$, and found the catalytic activities to he the same on all these surfaces, the HOR being controlled by rate-limiting dissociative adsorption of H_2, the ΔH being ~10 kJ mol^{-1}. The lack of any alloying effect was traced to the outer surfaces of these alloy electrodes remaining mainly Pt.

Studies on ternary catalysts of Pt (i.e. Pt–Fe–Cf, Pt–Fe–Mn, Pt–Fe–Mn, Pt–Fe–Co, Pt–Fe–Ni and Pt–Fe–Cu) supported on carbon in a PEM cell, at a Pt loading of 0.3 mg cm^{-2}, and at a temperature of 80 °C, showed, however, improved cell performance with alloys compared with pure Pt. This effect was attributed by the authors [108] to the increase in the ratio of strongly bonded H on Pt alloys to the total surface area.

Rao and Ray examined Pt–Au [109] and Pt–Ru [110] alloys in 0.5 H_2SO_4 at 27°C and found the activity for the HOR to be a maximum at 35% at Au and at 25% Ru, respectively.

Overall, there seems to be no dispute regarding the mechanism of HOR on Pt and Pt-alloys being rate-determining dissociative adsorption of H_2, after allowance for diffusion of H_2, although differences in activity were reported [108]. This is a likely consequence of the structure of the electrode employed in the investigation, and of temperature and Pt loading.

10.3. CO-tolerant HOR catalysts

Because of the importance of the HOR in fuel-cells, various Pt-based catalysts have been examined from the viewpoint of immunity of the electrocatalysis of the HOR from CO-poisoning of the anode catalysts.

Pure hydrogen is the ideal fuel for the HOR if optimal performance of low-temperature fuel-cells is to be realized. However, the H_2 produced from steam reforming or partial oxidation routes [see [111]] has an adverse influence on the kinetics of anodic oxidation of H_2, as it contains CO which poisons [112–114] the Pt anode catalyst even at a 10 ppm level, decreasing the cell performance by 0.2–0.3 V at 0.8 A cm^{-2}.

Fig. 19 illustrates the typical effect of CO on the performance of the Pt anode in a fuel-cell. The CO poisoning of Pt has been ascribed to the preferential adsorption of CO on Pt sites, as the Pt–CO bond-strength is greater than that of the Pt–H [115], so that CO inhibits the dissociative absorption of H_2 on Pt and its subsequent oxidation. The anodic current-density at low anode potentials under these conditions is written

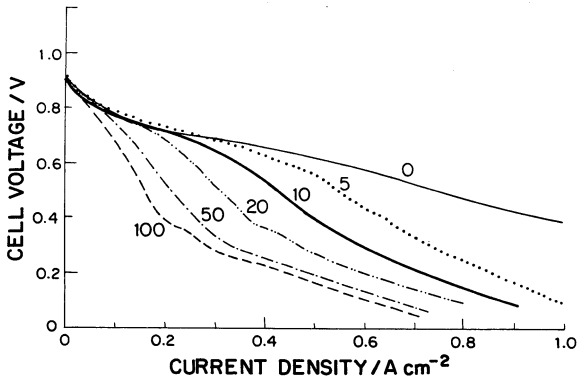

Fig. 19. Effect of CO level (ppm) in the H_2 feed on performance of a PEFC at 80 °C. Electrodes were based on an ionomer-impregnated Pt/C catalyst and thin, sputtered Pt film loading of 0.4 mg Pt per cm^2 (from ref. [101]. Reproduced with permission of the publishers).

as:

$$i = Fkp_{H_2}(1-\theta_{CO})^2 \quad (19)$$

assuming the adsorption process to be:

$$Pt + CO \rightarrow Pt\text{–}CO \quad (20)$$

and the H_2 dissociation to require two adjacent sites:

$$H_2 + 2Pt \xrightarrow{k} 2Pt\text{–}H \quad (21)$$

$$Pt\text{–}H \rightarrow Pt + H^+ + e \quad (22)$$

coupled with

$$Pt\text{–}CO + HO_{ads} \rightarrow Pt + CO_2 + H^+ + e \quad (23)$$

Adsorption of CO occurs (Eq. (20)) in parallel with process and hydrogen oxidation proceeds via processes (21) and 22 and, the simultaneous path being the oxidation of CO to CO_2, following process (23). Therefore, a limiting current-density behaviour can arise during the course of the HOR in the presence of CO.

Whether or not the H_2 oxidation current is proportional to $(1-\theta_{CO})^2$ appears to be a matter of debate, since RDE studies by Igarashi et al. [116] show that the current is proportional to $(1-\theta_{CO})$. These authors suggest that the adsorbed CO molecules are linearly bonded in a close-packed arrangement on the Pt surface, resulting in Pt sites which are completely isolated and on which dissociative adsorption is not favoured.

Kita et al. [117] found three adsorbed states of CO on Pt exhibiting different reactivities, but in situ IR spectra revealed only singly bonded and bridged CO. More investigations are needed to characterize the nature of the CO-bonding Pt sites in order to develop a new generation of HOR catalysts, based on Pt. Three strategies are currently being pursued to mitigate the influence of CO on the HOR. These include bleeding of O_2 into the H_2 fuel, operating the cell at elevated

Table 3
Kinetic data on CO-tolerant catalysts

Catalyst	Tafel slope (mV)		Reaction order (with respect to CO)	Reference
	In the absence of CO	In 100% CO		
Pt_{50} (0.5 M H_2SO_4)		70 ~ 80		
Pt_3Sn (0.5 M H_2SO_4)		220	Positive	[120]
$Pt_{75}Re_{25}$ (0.5 M H_2SO_4)		80	0.5	[119]
$Pt_{50}Ru_{50}$ (1 M H_2SO_4)	54			[119]
Pt (1 M H_2SO_4)	52			[119]
Pt–Mo (3:1); (1 M H_2SO_4)	50			[119]
Pt–Mo (4:1); (1 M H_2SO_4)	53			[119]
Pt–Mo (5:1); (1 M H_2SO_4)	52			[119]
Pt/C/Nafion	20–30		−0.39	[109]
Pt–Rn/Nafion	20–30		−0.46	[109]
Pt–Sn/C/Nafion	20–30		−0.88	[109]

temperatures and use of Pt-alloys which are CO-tolerant for H_2 oxidation (see Table 3).

Oxygen bleeding, originally proposed in the 1990s, involved injection of 0.4–2% O_2 into the CO-contaminated H_2 stream to oxidize the CO adsorbed on the catalyst [112–118]. A related technique is the oxidative removal of CO by nascent O_2 from H_2O_2, which is introduced in the humidification system [109].

Operation of fuel-cells at temperatures above 150 °C would diminish CO adsorption on Pt catalysts versus adsorption of H, and, therefore, its adverse influence on the performance of the Pt anode [119–121]; this concept has indeed been demonstrated in phosphoric acid fuel-cells. However, implementation in PEM fuel-cells requires development of membranes that are stable in the temperature range of 120–200 °C.

Most efforts have been directed to developing CO-tolerant Pt alloys or composites (Fig. 20), based on the concept of so-called 'bifunctional catalysis' that provide

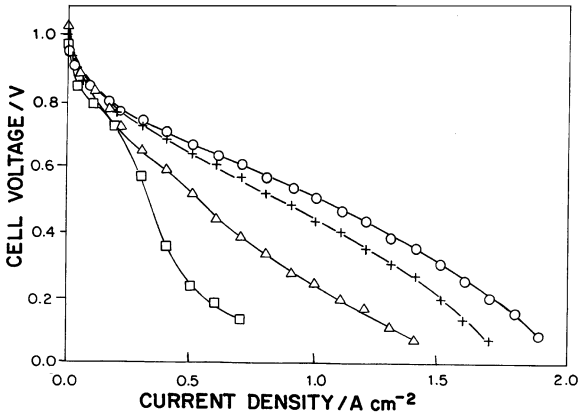

Fig. 20. Performance of a 5 cm^2 fuel-cell with H_2/CO (100 ppm) and O_2 at 85 °C using various anode catalysts: □ Pt/C; △ PtRu/C; + PtMo/C; data for Pt/C with H_2/O_2 are shown (○) for comparison. (From ref. [118]. Reproduced by permission of the publishers).

some sites at which CO can be oxidized along with others where H_2 dissociative chemisorption can take place. Examples are found where a second element is introduced, e.g. Ru [120–123], Sn [109,124–126], Rh [127], Mo [120,128–130], Re [131], WO_3 [132], that is either alloyed or co-deposited. Another interesting catalyst is the Pd–Au alloy [133]. The primary focus of these investigations is towards realizing high activity for the HOR in the presence of CO. Mechanistic and kinetic studies related to the HOR on these Pt alloy catalysts are, however, few.

Table 3 provides a limited compilation of such kinetic data on the CO-tolerant Pt alloy catalysts. The results show that the slow-step in the HOR on these substrates is the reverse of either process (I) or (II). However, the Tafel slope values at Pt–Re in the presence of CO defy explanation, while the b value of 80 mV can be attributed to the electrochemical oxidation following process 24. The HOR is nevertheless assumed to processed in the same way with or without CO in the H_2. Polarization data in Fig. 20 show no limiting currents for the HOR at two binary catalysts, unlike on Pt, and this current–voltage pattern is considered to arise on account of simultaneous oxidation of H_2 and CO. CO oxidation is believed to be facile on oxophilic materials [122] such as Ru, Sn or Mo, having surface OH states, which electrochemically convert CO to CO_2, which is desorbed thereby providing Pt sites available for the HOR.

Of all the catalysts examined so far, Pt–Mo is the most promising since CO oxidation proceeds at potentials as low as 0.1 V [129]. Voltammetric studies, complemented by in situ X-ray absorption near-edge structure measurements at the Mo K-edge indicate redox participation of oxy-hydroxides of Mo as mediator states in the oxidation of CO. In situ FTIR spectroscopic studies [92,111–115] have shown that CO bonding is both linear and bridged. However, CO

is bound linearly on Pt–Ru and Pt–Sn alloys. CO oxidation depends not only on the composition of the catalyst but also on the nature of the bonding of CO to the Pt sites. On Pt–Mo alloys, CO, linearly adsorbed on Pt sites, is oxidized at ~ 0.1 V by a redox-mediated mechanism and at high overpotentials, by the OH species on Pt. At low overpotentials, oxidation of CO to CO_2 releases 'hole' Pt sites for oxidation of H_2. In the case of Pt–Ru alloys, the surface OH groups on Ru sites permit oxidation of CO of high potentials (0.47 V vs. NHE), and the Sn sites in Pt–Sn alloys permit oxidation at CO at ~ 0.03 V. However, Pt–Sn alloys are unstable at elevated temperatures.

A novel colloidal Pd–Au/C catalyst, evaluated recently [133], is $Pd_{0.8}Au_{0.8}$ on Vulcan XC-72 carbon, exhibited superior activity compared with the Pt–Ru catalyst at CO levels of 250 and 1000 ppm. This was explained in the terms of low steady-state coverage by CO on PdAu (vs. PtRu), which provided relatively more Pt sites for the HOR to proceed, a view supported by temperature-programmed desorption experiments at Pd–Au alloys.

References

[1] J. Tafel, Zeit fur Phys. Chem. 50 (1905) 641.
[2] J. Tafel, N. Naumann, Ber. der Deutschen. Chemischen Gerellschaft 34 (1901) 3291.
[3] J. Tafel, O. Rosenheim, F. During, G. Fenner, Liebig's Ann. der Chimie A301 (1898) 285.
[4] K.F. Bonhöffer, Zeit fur Phys. Chem. 113 (1924) 213.
[5] W. Nicholson, A. Carlisle, Nicholson's J. 4 (1800) 183.
[6] B.E. Conway, H.A. Kozlowska, H.P. Dhar, Electrochim. Acta 19 (1974) 439.
[7] A.N. Frumkin, B. Slygin, Acta Physicochim., URSS, (1933).
[8] F.G. Will, C.A. Knorr, Zeit. Elektrochem. 64 (1960) 258.
[9] M.W. Breiter, Electrochim. Acta 8 (1963) 925.
[10] J. Clavilier, J.M. Orts, R. Gomez, J.M. Fliu, A. Aldaz, in: B.E. Conway, G. Jerkiewicz (eds.), Proceedings of Symposium on Electrochemistry and Materials Science, in Proceedings of Cathodic H Absorption and Adsorption, vol. 94–21, The Electrochemical Society Inc., Pennington, NJ (1995), 167.
[11] J. Clavilier, A. Rodes, K.E. Achi, M.A. Zamakhchan, J. Chim. Phys. 88 (1991) 1291.
[12] M. Boudart, J. Am. Chem. Soc. 72 (1952) 3566.
[13] K. Christmann, in: J. Lipkowski, P.N. Ross (Eds.), Electrocatalysis (Chapter 1), Wiley-VCH, New York, 1998.
[14] M.H. Breiter, W. Böld, Zeit. Elektrochem. 64 (1960) 897.
[15] G. Jerkiewicz, A. Zolfaghari, J. Electroanal. Chem. 467 (1999) 177.
[16] P.N. Ross, in: G. Vanselow, R. Howe (Eds.), Chemistry and Physics of Solid Surfaces, vol. VI, Springer, New York, 1982, p. 173.
[17] R.R. Adzic, F. Feddix, B.Z. Nikolic, E. Yeager, J. Electroanal. Chem. 341 (1992) 287.
[18] J. Barber, S. Morin, B.E. Conway, J. Electroanal. Chem. 446 (1998) 125.
[19] P.N. Ross, Surf. Sci. 102 (1981) 463.
[20] A. Bewick, J.W. Russell, J. Electroanal. Chem. 132 (1982) 329.
[21] F.G. Will, J. Electrochem. Soc. 112 (1965) 451.
[22] M.W. Breiter, Ann. New York Acad. Sci. 101 (1963) 709.
[23] J.G. Aston, J. Phys. Chem. 67 (1963) 2042.
[24] A.T. Hubbard, R. Isishkawa, J. Katakaru, J. Electroanal. Chem. 86 (1978) 271.
[25] R. McCabe, L. Schmidt, Proceedings of 7th International Vacuum Congress and joint 3rd International Conference on Solid Surfaces, Vienna, 1977, p. 1201.
[26] K. Christmann, G. Ertl, Surf. Sci. 60 (1976) 365.
[27] C. Kemball, Proc. R. Soc. London A 187 (1946) 73.
[28] B.E. Conway, H.A. Kozlowska, W.B.A. Sharp, J. Chem. Soc. Faraday Trans., I 74 (1978) 1373.
[29] D.P. Wilkinson, B.E. Conway, Electrochim. Acta 38 (1993) 997.
[30] G. Jerkiewicz, A. Zolfaghari, J. Electrochem. Soc. 143 (1996) 1240.
[31] B.E. Conway, H.A. Kozlowska, F.C. Ho, J. Vac. Sci. Technol. 14 (1977) 351.
[32] B.E. Conway, H.A. Kozlowska, Accts. Chem. Res. 14 (1981) 49.
[33] B.E. Conway, E. Gileadi, Trans. Faraday Soc. 58 (1962) 2493.
[34] B.E. Conway, in: A. Wieckowski (Ed.), Interfacial Electrochemistry (Chapter 9), Marcel Dekker, New York, 1999.
[35] M. Ehsasi, K. Christmann, Surf. Sci. 194 (1988) 172.
[36] K. Christmann, O. Schober, G. Ertl, M. Neamann, J. Chem. Phys. 60 (1974) 4528.
[37] N. Furuya, S. Motoo, J. Electroanal. Chem. 78 (1977) 243.
[38] B.E. Conway, G. Jerkiewicz, Electrochim. Acta 45 (2000) 4075.
[39] N.M. Markovic, S.T. Sarraf, H.A. Gasteiger, P.N. Ross, J. Chem. Soc. Faraday Trans. 92 (1996) 3719.
[40] N.M. Markovic, B.N. Grgur and P.N. Ross, J. Phys. Chem. B.C. (1997).
[41] J. Horiuti, T. Toya, in: M. Green (Ed.), Solid-State Surface Science, Marcel Dekker, New York, 1969.
[42] R. Simpraga, J. Electroanal. Chem. 355 (1993) 79.
[43] B.E. Conway, L. Bai, J. Chem. Soc. Faraday Trans., I 81 (1985) 1841.
[44] J. O'M. Bockris, in: J. O'M. Bockris, B.E. Conway (Eds.), Modern Aspects of Electrochemistry, vol. 1 (Chapter 4), Butterworths Sci. Publications, London, 1954.
[45] B.E. Conway, B.V. Tilak, in: D.D. Eley, H. Pines, P.B. Weisz (Eds.), Chapter 1 in Advance in Catalysis, vol. 38, Academic Press Inc., New York, 1992.
[46] N.D. Lang, W. Kohn, Phys. Rev. B 7 (1973) 3541.
[47] J.P. Badiali, Electrochim. Acta 31 (1986) 149.
[48] B.E. Conway, B.V. Tilak, Adv. Catal. 38 (1992) 1.
[49] L. Bai, D.A. Harrington, B.E. Conway, Electrochim. Acta 32 (1987) 1713.
[50] M. Enyo, J. Res. Inst. Catalysis, Hokkaido Univ., 25 (1977) 17.
[51] M. Enyo, in: B.E. Conway, J.O'M. Bockris, E.B. Yeager, S.U.M. Khan, R.E. White (Eds.), Comprehensive Treatise of Electrochemistry (Chapter 5), Plenum Press, New York, 1983, p. 241.
[52] B.V. Tilak, C.G. Rader, B.E. Conway, Electrochim. Acta 22 (1977) 1167.
[53] B.E. Cownay, in: B.E. Conway, R.E. White, J.O'M. Bockris (Eds.), Modern Aspects of Electrochemistry, vol. 16, Plenum Press, New York, 1985, p. 103.
[54] (a) B.V. Tilak, S. Venkatesh, S.K. Rangarajam, J. Electrochem. Soc. 136 (1989) 1977;
(b) A. Lasia, J. Electroanal. Chem. 454 (1998) 115;
(c) J.N. Agar, Discuss. Faraday Soc. 1 (1947) 84.
[55] B.E. Conway, D. MacKinnon, B.V. Tilak, J. Chem. Soc. Trans. Faraday Soc. 66 (1970) 1023.
[56] E.B. Yeager, D. Scherson, Extended Abstracts of the Spring Meeting of the Electrochem. Soc., San Francisco, CA, 1983, p. 1043.
[57] B.E. Conway, R. Brousseau, unpublished; see R. Brousseau, Ph.D. thesis, University of Ottawa, 1989.
[58] B.E. Conway, L. Bai, D.F. Tessier, J. Electroanal. Chem. 161 (1984) 39.

[59] L. Bai, B.E. Conway, J. Chem. Soc. Faraday Trans. 1 (81) (1985) 1841.
[60] J.A.V. Butler, M. Armstrong, J. Chem. Soc., London (1934) 743.
[61] D.A. Harrington, B.E. Conway, J. Electroanal. Chem. 221 (1987) 1.
[62] A. Bewick, K. Kunimatsu, J. Robinson, J.W. Russell, J. Electroanal. Chem. 119 (1981) 175.
[63] A. Bewick, K. Kunimatsu, B.S. Pons, Electrochim. Acta 25 (1975) 405.
[64] A. Bewick, K. Kunimatsu, Surf. Sci. 101 (1980) 131.
[65] R.J. Nichols, A. Bewick, J. Electroanal. Chem. 243 (1988) 445.
[66] R.J. Nichols, in: J. Lipkowski, P.N. Ross (Eds.), Adsorption of Molecules at Metal Electrodes (Chapter 7), VCH, New York, 1992.
[67] G.M. Torrie, G.N. Patey, Electrochim. Acta 36 (1991) 1677.
[68] H. Lei, B. Wu, C. Cha, J. Electroanal. Chem. 332 (1992) 257.
[69] J. Clavilier, J.M. Feliu, A. Fernandez-Viga, A. Aldaz, J. Electroanal. Chem. 294 (1990) 193.
[70] B.E. Conway, L. Bai, J. Electroanal. Chem. 198 (1986) 149.
[71] H. Ogasawara, M. Ito, Chem. Phys. Lett. 221 (1994) 213.
[72] N. Nanbu, F. Kitamura, T. Ohsaka, K. Tokuda, J. Electroanal. Chem. 485 (2000) 128.
[73] M. Jaksic, Int. J. Hydrogen Energy 12 (1987) 727.
[74] A. Azzam, B.E. Conway, J. O'M. Bockris, H. Rosenberg, Trans. Faraday Soc. 46 (1950) 918.
[75] B.E. Conway, W.B.A. Sharp, H.A. Kozlowska, E. Criddle, Anal. Chem. 45 (1973) 1331.
[76] H. Angerstein-Kozlowska, in: J.O'M Bockris, E. Yeager, B.E. Conway (Eds.), Comprehensive Treatise in Electrochemistry, vol. 9 (Chapter 2), Plenum Publ. Co, New York, 1984.
[77] S. Trasatti, J. Electroanal. Chem. 39 (1977) 183.
[78] B.E. Conway, Electrochemical Data, Elsevier Publ. Co, Amsterdam, 1952.
[79] A.N. Frumkin, P. Dolin, B.V. Erschler, Acta Physicochim. URSS.
[80] M. Breiter, J. Electroanal. Chem. 7 (1964) 38.
[81] J. Barber, B.E. Conway, J. Electroanal. Chem. 461 (1999) 80.
[82] J. Barber, S. Morin, B.E. Conway, J. Electroanal. Chem. 446 (1998) 1109.
[83] B.E. Conway, G. Jerkiewicz, Electrochim. Acta 42 (2000) 4075.
[84] H. Kita, J. Res. Inst. Catalysis, Hokkaido Univ., 13 (1965) 151.
[85] B.E. Conway, J.O'M. Bockris, J. Chem. Phys. 26 (1957) 232.
[86] D.A. Petrii, G.A. Tserlina, Electrochim. Acta 39 (1994) 1739.
[87] (a) J.O'M. Bockris, E.C. Potter, J. Chem. Phys. 19 (1952) 471;
(b) J.O'M. Bockris, E.C. Potter, J. Electrochem. Soc. 99 (1952) 169.
[88] B.E. Conway, Electrochemical Data (Chapter X), Elsevier Publ. Co, Amsterdam, 1952.
[89] R. Parsons, Trans. Faraday Soc. 34 (1958) 1053.
[90] M. Jaksic, Electrochim. Acta 45 (2000) 4085.
[91] B.E. Conway, L. Bai, M.A. Sattar, Intl. J. Hydrogen Energy 9 (1987) 607.
[92] H.A. Kozlowska, B.E. Conway, J. Electroanal. Chem. 95 (1979) 1.
[93] S.Y. Qian, B.E. Conway, G. Jerkiewicz, Int. J. Hydrogen Energy 25 (2000) 539.
[94] B.E. Conway, L. Bai, J. Electroanal. Chem. 198 (1986) 149.
[95] R.J. Mannan, Ph.D. thesis, Chemistry, University of Pennsylvania, 1967.
[96] W. Vogel, J. Lundquist, P. Ross, P. Stonehart, Electrochim. Acta 20 (1975) 79.
[97] M.J. Croissant, T. Napporn, J.M. Leger, C. Lamy, Electrochim. Acta 43 (1998) 2447.
[98] K. Mund, G. Richter, R. Shulte, F.V. Sturn, Z. Electrochem. 77 (1973) 839.
[99] F.V. Sturm, in: J.E.D. McIntyre, S. Srinivasan, F.G. Will (Eds.), Electrode Materials and Processes for Energy Conversion and Storage, vols. 77-6, The Electrochemical Society Inc, Princeton, NJ, 1977, p. 247.
[100] V.S. Bagotzki, N.V. Osetrova, J. Electroanal. Chem. 43 (1973) 233.
[101] P.N. Ross, P. Stonehart, J. Res. Inst. Catal, Hokkaido Univ., 22 (1974) 22.
[102] N.A. Urrison, G.V. Shteinburg, V.S. Bagotskii, Electrokhimiya 11 (1975) 1298.
[103] S. Shibata, M.P. Sumino, Electrochim. Acta 16 (1971) 1511.
[104] N.V. Osetrova, V.S. Bagotskii, Electrokhimiya 9 (1973) 1325.
[105] M.W. Breiter, Electrochim. Acta 7 (1962) 601.
[106] R.M.Q. Mello, E.A. Ticianelli, Electrochim. Acta 42 (1997) 1031.
[107] S. Mukherjee, J. McBreen, J. Electrochem. Soc. 143 (1996) 2285.
[108] J. Shim, D.-Y. Yoo, J.S. Lee, Electrochim. Acta 45 (2000) 1943.
[109] K.V. Rao, C.B. Roy, Ind. J. Chem. 19A (1980) 834.
[110] K.V. Rao, C.B. Roy, Ind. J. Chem. 21A (1982) 34.
[111] B.V. Tilak, S. Srinivasan, in: L.C. Wilbur (Ed.), Handbook of Energy Systems Engineering, Wiley, NY, 1985, p. 1459.
[112] S. Gottesfield, J. Pafford, J. Electrochem. Soc. 135 (1988) 2651.
[113] H.F. Oetjen, V.M. Schmidt, U. Stimming, F. Trila, J. Electrochem. Soc. 143 (1996) 3838.
[114] S. Gottesfeld, T.A. Zawodzinski, in: R.C. Alkire, H. Gerisher, D.M. Kolb, C.W. Tobias (Eds.), Advances in Electrochemical Science and Engineering, vol. 5, Wiley-VCH, New York, 1997, p. 197.
[115] J.B. Benziger, in: E. Shustorovich (Ed.), Reaction Energetics on Metal Surfaces; Theory and Applications, ECH, New York, 1992, p. 53.
[116] H. Igarashi, T. Fijino, M. Watanabe, J. Electroanal. Chem. 391 (1995) 119.
[117] H. Kita, H. Naohara, T. Nakato, S. Taguchi, A. Aramata, J. Electroanal. Chem. 386 (1995) 197.
[118] M.S. Wilson, T.E. Springer, T.A. Zawodzinski, S. Gottesfeld, Proceedings of 28th Intersociety Energy Conservation Engineering Conference, vol. 1, Atalnta, Georgia, 1993, p. 1203.
[119] S. Gottesfeld, Paper Presented at the DOE Review Meeting, Washington, DC, 1998.
[120] S.J. Lee, S. Mukerjee, E.A. Ticianelli, J. McBreen, Electrochim. Acta 44 (1999) 3283.
[121] C. Vickers, Proceedings of Fuel Cell Seminar, Orlando, Florida, November 1996.
[122] H. Gasteiger, N. Markovic, P. Ross, J. Phys. Chem. 99 (1995) 8290.
[123] T.J. Schmidt, H. Gasteiger, R.J. Behm, J. Electrochem. Soc. 146 (1999) 1296.
[124] H. Gasteiger, N. Markovic, P. Ross, J. Phys. Chem. 99 (1995) 8945.
[125] M. Watanabe, M. Shibata, S. Motoo, J. Electroanal. Chem 187 (1985) 161.
[126] M. Shibata, N. Furuya, J. Electroanal. Chem. 269 (1989) 217.
[127] P.N. Ross, Jr., K. Kinoshita, A.J. Scarpellino, P. Stonehart, J. Electroanal. Chem. 59 (1975) 177.
[128] (a) B. Grgur, G. Zhuang, N. Markovic, P. Ross, J. Phys. Chem. B 100 (1997) 19538;
(b) B. Grgur, G. Zhuang, N. Markovic, P. Ross, J. Phys. Chem. B 101 (1977) 3910;
(c) B. Grgur, G. Zhuang, N. Markovic, P. Ross, J. Phys. Chem. B 102 (1998) 2494.
[129] S. Mukerjee, S.J. Lee, E.A. Ticianelli, J. McBreen, B.N. Grger, N.M. Markovic, P.N. Ross, J.R. Giallombardo, E.S. DeCatro, Electrochem. Solid-State Lett. 2 (1) (1999) 12.

[130] A. Pozio, L. Giorgi, E. Antolini, E. Passalaqua, Electrochim. Acta 46 (2000) 555.
[131] B.N. Grgur, N.M. Markovic, P.N. Ross, Electrochim. Acta 43 (1998) 3631.
[132] A.C.C. Tseung, P.K. Shen, K.Y. Chen, J. Power Sources 61 (1996) 223.
[133] T.J. Schmidt, Z. Jusys, H.A. Gasteiger, R.J. Behm, U. Endruschat, H. Boennemann, J. Electroanal. Chem. 501 (2001) 132.